Journal of Quantitative Spectroscopy & Radiative Transfer 151 (2015) 310–326

Contents lists available at ScienceDirect

Journal of Quantitative Spectroscopy & Radiative Transfer

journal homepage: www.elsevier.com/locate/jqsrt

Absorption and scattering by fractal aggregates and by their equivalent coated spheres

Razmig Kandilian, Ri-Liang Heng, Laurent Pilon *

Mechanical and Aerospace Engineering Department, Henry Samueli School of Engineering and Applied Science, University of California, Los Angeles, Los Angeles, CA 90095, USA

ARTICLE INFO

Article history:
Received 3 September 2014
Received in revised form
14 October 2014
Accepted 23 October 2014
Available online 1 November 2014

Keywords:
Scattering
Fractal aggregates
Superposition T-matrix
Equivalent particle
Coated sphere

ABSTRACT

This paper demonstrates that the absorption and scattering cross-sections and the asymmetry factor of randomly oriented fractal aggregates of spherical monomers can be rapidly estimated as those of coated spheres with equivalent volume and average projected area. This was established for fractal aggregates with fractal dimension ranging from 2.0 to 3.0 and composed of up to 1000 monodisperse or polydisperse monomers with a wide range of size parameter and relative complex index of refraction. This equivalent coated sphere approximation was able to capture the effects of both multiple scattering and shading among constituent monomers on the integral radiation characteristics of the aggregates. It was shown to be superior to the Rayleigh–Debye–Gans approximation and to the equivalent coated sphere approximation proposed by Latimer. However, the scattering matrix element ratios of equivalent coated spheres featured large angular oscillations caused by internal reflection in the coating which were not observed in those of the corresponding fractal aggregates. Finally, the scattering phase function and the scattering matrix elements of aggregates with large monomer size parameter were found to have unique features that could be used in remote sensing applications.

1. Introduction

Particle aggregation and coagulation is a frequent occurrence in numerous applications such as combustion systems [1], atmospheric science [2,3], astronomy and astrophysics [4], chemistry [5], and biotechnology [6–8]. Small particles aggregate to form fractal-like structures changing the light absorption and scattering properties of the suspension [2]. For example, Fig. 1a, b, c, d, e, and f shows micrographs of soot [9], snow [10], cosmic dust [11], gold nanoparticles [12], bacteria [13], and microalgae aggregates, respectively. In all these systems, knowledge of the radiation characteristics of the fractal aggregates are of prime importance for radiation transfer analysis and remote sensing applications. The radiation characteristics of soot and aerosol aggregates have been studied extensively as reviewed by Sorensen [2]. However, to the best of our knowledge, those pertaining to aggregates composed of larger monomers such as microalgae colonies have not been studied.

Microalgae are single cell photosynthetic microorganisms growing in freshwater or seawater. They can be grown in photobioreactors (PBRs) exposed to solar radiation to produce biofuels as well as various pharmaceuticals and biochemicals [14]. For example, *Botryococcus braunii* (Fig. 1f) can be used for producing biofuels for powering jet engines [14]. This species secretes exopolysaccharides (EPS), a viscous substance coating the cell surface and causing their aggregation into colonies. EPS production is part of a protection mechanism activated in response to environmental conditions such as limited

* Corresponding author. Tel.: +1 310 206 5598; fax: +1 310 206 4830.
E-mail address: pilon@seas.ucla.edu (L. Pilon).
URL: http://www.seas.ucla.edu/~pilon/ (L. Pilon).

http://dx.doi.org/10.1016/j.jqsrt.2014.10.018
0022-4073/

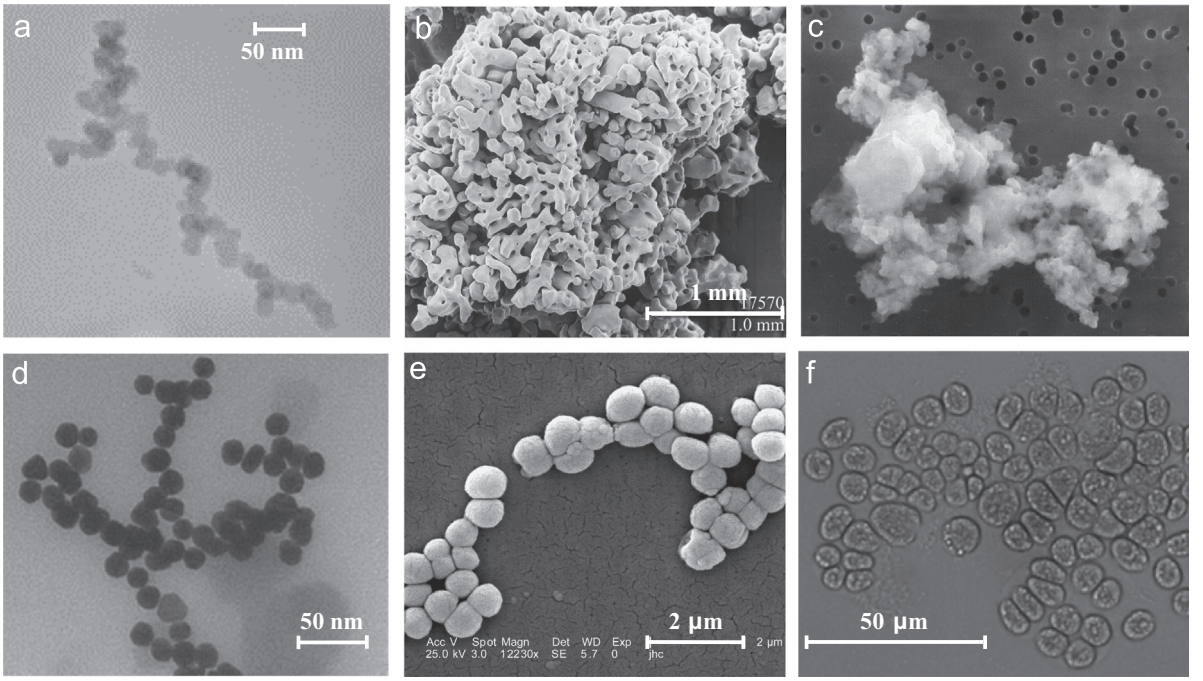

Fig. 1. Micrographs of fractal aggregates of (a) soot [9], (b) snow [10], (c) cosmic dust [11], (d) gold nanoparticles [12], (e) the bacteria *M. luteus* [13], and (f) colonie of the microalgae *B. braunii*.

illumination [15], non-optimal temperature [16], high salinity [16], and limited nutrient availability [17]. In addition, a recent study demonstrated reversible cell aggregation in concentrated *Chlorella vulgaris* cultures used for protein, starch, and lipid production [18]. The authors hypothesized that aggregation occurred at large cell concentration due to the proximity of the cells to one another. Since larger microalgae cells possess a larger surface charge density compared to smaller cells, the electrostatic repulsion between larger cells is much stronger than that between a large and a small cell [18]. This leads to aggregation of the smaller cells in the space created by the electrostatic repulsion between the larger cells.

To achieve maximum biomass and biofuel productivities, light transfer in the PBRs must be optimized [19–21]. For example, a flat-plate PBR should be designed and operated such that the fluence rate at the backwall corresponds to the photosynthetic compensation point, i.e., the minimum amount of energy required to maintain cell metabolism [21]. The latter was reported to be 10 $\mu mol_{h\nu}/m^2$ s for the microalgae *Chlamydomonas reinhardtii* [22] and 2 $\mu mol_{h\nu}/m^2$ s for the cyanobacteria *Arthrospira platensis* [19]. Optimizing PBRs for maximum biomass productivity requires the solution to the radiative transfer equation and the knowledge of the absorption and scattering cross-sections as well as the scattering phase function of the microalgal suspension [20]. Moreover, the scattering matrix elements of the microalgal suspension may be measured for remote sensing of the PBR [23]. The radiation characteristics of suspensions composed of single cells can be predicted theoretically [24–27] or measured experimentally [20,28]. However, theoretical or experimental characterization of the radiation characteristics of suspensions consisting of microalgae colonies have received less attention.

Several numerical methods exist to estimate the radiation characteristics of aggregates consisting of spherical monomers. They include the superposition T-matrix method [29], the generalized multiparticle-Mie theory [30], and the volume integral method [31]. However, depending on the size of the aggregate, calculations can be time consuming and require significant computational resources [4]. Thus, it would be computationally far more efficient to approximate the radiation characteristics of aggregates with complex morphology by those of particles with simple shapes such as spheres, coated spheres, or cylinders whose radiation characteristics can be computed relatively rapidly [32]. For example, Drolen and Tien [33] approximated the absorption and scattering cross-sections of soot particle aggregates as those of a volume equivalent solid sphere. More recently, Lee and Pilon [34] demonstrated that the absorption and scattering cross-sections per unit length of randomly oriented linear chains of spheres can be approximated as those of randomly oriented infinitely long cylinders with equivalent volume per unit length. Alternatively, the Rayleigh–Debye–Gans (RDG) approximation provides an analytical expression for the absorption and scattering cross-sections and the scattering phase function of aggregates based on the assumption that the size of the monomers is much smaller than the incident radiation wavelength [35].

This study aims to identify approximations and equivalent particles for rapidly and accurately predicting the absorption and scattering cross-sections and, if possible, the scattering matrix elements of fractal aggregates composed of relatively large monodisperse or polydisperse optically soft spherical monomers. The goal is to facilitate the predictions of radiation characteristics of fractal

aggregates with large monomers compared with the wavelength of the incident radiation where numerical methods are too time consuming and resource intensive for practical purposes.

2. Background

2.1. Modeling fractal aggregates

An ensemble of N_s monodisperse spherical monomers of radius a aggregated in a fractal structure satisfies the statistical rule given by [2]

$$N_s = k_f \left(\frac{R_g}{a}\right)^{D_f} \tag{1}$$

where R_g is the aggregate radius of gyration defined as the mean-squared of the distances between the aggregate center of mass and the geometric center of each particle. The constants D_f and k_f are the so-called fractal dimension and prefactor, respectively. For example, ordered linear chains of spheres (1D), square sheets (2D), and simple cubic (3D) aggregates have fractal dimensions D_f of 1.0, 2.0, and 3.0, respectively. On the other hand, fractal dimension D_f of random aggregates depends on the aggregation mechanism [2]. Aggregation by collisions due to Brownian motion can result in diffusion limited aggregation or in reaction limited aggregation [2]. In diffusion limited aggregation, particles collide and immediately stick to the surface of the aggregate [7]. These aggregates typically have fractal dimension D_f of 1.75–1.8 [7]. In reaction limited aggregation, particles may penetrate the aggregate when they collide without immediately sticking to the surface. These aggregates feature fractal dimension D_f equal to 2.2 [7]. In addition, Jackson et al. [8] experimentally found that the fractal dimension of phytoplanktonic suspensions ranged from 2.25 to 2.36. The prefactor k_f is typically treated as a fitting constant also known as the packing factor [7]. It has been reported to range between 1.2 and 3.0 for soot particles [35–38]. Sorensen [2] and Lapuerta [39] assumed a value of k_f for aggregates of soot particles to be 1.593 corresponding to the most compact packing of monodisperse monomers.

Fractal aggregate formation can be numerically simulated using particle cluster aggregation algorithm [2,40,41]. This method launches a spherical particle of radius a on a random walk. A collision between the marching particle and the aggregate leads to adherence of the two if the new aggregate structure satisfies the prescribed prefactor k_f and fractal dimension D_f [40]. This procedure is repeated until the aggregate contains the desired number of monomers N_s.

2.2. Scattering matrix

The Stokes vector is composed of the four Stokes parameters I, Q, U, and V describing the intensity and degree of polarization of an electromagnetic wave [42]. For a given aggregate whose center of mass is located at the origin of a spherical coordinate system, the far-field scattered intensity at location $\mathbf{r}$ in direction $\hat{s}$ is denoted by $\mathbf{I_{sca}}(\mathbf{r},\hat{s}) = (I_{sca}, Q_{sca}, U_{sca}, V_{sca})^T$ can be related to the incident irradiance $\mathbf{I_{inc}}(\hat{s}_i) = (I_{inc}, Q_{inc}, U_{inc}, V_{inc})^T$ by the Mueller matrix $[Z(\Theta)]$ according to [29]

$$\mathbf{I_{sca}}(\mathbf{r},\hat{s}) = \frac{1}{r^2}[Z(\Theta)]\mathbf{I_{inc}}(\hat{s}_i) \tag{2}$$

Here, r is the norm of the location vector $\mathbf{r}$ corresponding to the distance between the particle and the observation point. The scattering angle Θ is defined as the angle between the incident $\hat{s}_i$ and the scattered $\hat{s}$ directions. For randomly oriented aggregates, it is more convenient to use the normalized scattering, or Stokes, matrix $[F(\Theta)]$ given by [43]

$$[F(\Theta)] = \frac{4\pi}{\langle C^a_{sca}\rangle}[Z(\Theta)] \tag{3}$$

where $\langle C^a_{sca}\rangle$ is the orientation-averaged scattering cross-section of the aggregate. It is defined as the fraction of the unpolarized radiant energy incident on the surface of the randomly oriented aggregate that is scattered in any direction [44]. Similarly, the orientation-averaged absorption cross-section $\langle C^a_{abs}\rangle$ represents the fraction of the unpolarized radiant energy incident on the surface of the aggregate that is absorbed [44]. The orientation-averaged extinction cross-section $\langle C^a_{ext}\rangle$ is defined as the sum of the absorption and scattering cross-sections, i.e., $\langle C^a_{ext}\rangle = \langle C^a_{abs}\rangle + \langle C^a_{sca}\rangle$ [44]. For randomly oriented aggregates with a plane of symmetry, the scattering matrix $[F(\Theta)]$ can be expressed as [44]

$$[F(\Theta)] = \begin{bmatrix} F_{11}(\Theta) & F_{21}(\Theta) & 0 & 0 \\ F_{21}(\Theta) & F_{22}(\Theta) & 0 & 0 \\ 0 & 0 & F_{33}(\Theta) & F_{34}(\Theta) \\ 0 & 0 & -F_{43}(\Theta) & F_{44}(\Theta) \end{bmatrix} \tag{4}$$

The asymmetry factor of an aggregate is defined as [42]

$$g = \frac{1}{4\pi}\int_{4\pi} F_{11}(\Theta)\cos\Theta\, d\Omega \tag{5}$$

It is equal to 0, 1, and -1 for isotropic, purely forward, and purely backward scattering, respectively [44]. In addition, the Henyey–Greenstein (HG) approximate phase function is often used in radiative transfer analysis for its simplicity as it predicts $F_{11}(\Theta)$ only as a function of the asymmetry factor g according to [45]

$$F_{11,HG}(\Theta) = \frac{1-g^2}{[1+g^2-2g\cos\Theta]^{3/2}} \tag{6}$$

Several analytical and numerical methods exist for predicting the absorption and scattering cross-sections of aggregates as well as their scattering matrix elements as discussed in the following sections.

2.3. The Rayleigh–Debye–Gans (RDG) approximation

Monomers of radius a in a given aggregate are characterized by (i) their size parameter defined as $\chi_s = 2\pi a\lambda^{-1}$ where λ is the wavelength of radiation in vacuum and (ii) their relative complex index of refraction $m = n + ik$ defined as the ratio of the complex indices of refraction of the monomers $m_s = n_s + ik_s$ and of the refractive index n_m of the non-absorbing surrounding medium [35]. The Rayleigh–Debye–Gans (RDG) approximation provides a closed-form analytical expression for absorption

and scattering cross-sections as well as for the scattering phase function of randomly oriented fractal aggregates [2,35,46]. It is valid for aggregates composed of optically soft monomers such that $|m-1| \ll 1$ with small size parameters, i.e., $\chi_s \ll 1$. Under these conditions, the aggregate absorption cross-section $\langle C^a_{abs,RDG}\rangle$ is the sum of the absorption cross-sections of all constituent monomers and is expressed as [2,35]

$$\langle C^a_{abs,RDG}\rangle = N_s \langle C_{abs,R}\rangle \tag{7}$$

Here, $\langle C_{abs,R}\rangle$ is the absorption cross-section of a single spherical monomer of size parameter χ_s given, in the Rayleigh scattering regime, by [35]

$$\langle C_{abs,R}\rangle = \frac{\lambda^2 \chi_s^3}{\pi} \mathrm{Im}\left(\frac{m^2-1}{m^2+2}\right). \tag{8}$$

Similarly, the aggregate scattering cross-section $\langle C^a_{sca,RDG}\rangle$ can be estimated by [2,35]

$$\langle C^a_{sca,RDG}\rangle = 2\pi N_s^2 \langle C_{sca,vv,R}\rangle \int_0^{\pi} \frac{1}{2} S\left(qR_g\right)\left(1+\cos^2\Theta\right)\sin\Theta\, d\Theta \tag{9}$$

where $\langle C_{sca,vv,R}\rangle$ represents the vertically polarized scattering cross-section for vertically polarized incident radiation [2,35]. For a monomer of size parameter χ_s in the Rayleigh scattering regime, $\langle C_{sca,vv,R}\rangle$ can be written as

$$\langle C_{sca,vv,R}\rangle = \frac{\lambda^2 \chi_s^6}{4\pi^2}\left|\frac{m^2-1}{m^2+2}\right|^2 \tag{10}$$

Here, $S(qR_g)$ is the scattering structure factor of the aggregates describing the intensity of scattered radiation as a function of the scattering wavevector $q = 4\pi\lambda^{-1}\sin(\Theta/2)$ [2]. For an aggregate of fractal dimension D_f and radius of gyration R_g, $S(qR_g)$ can be expressed as [46]

$$S\left(qR_g\right) = \left[1+\frac{8}{3}\frac{(qR_g)^2}{D_f}+(qR_g)^8\right]^{-D_f/8} \tag{11}$$

Note that, for very small and very large aggregates compared with the radiation wavelength, i.e., for $qR_g \ll 1$ and $qR_g \gg 1$, the structure factor simplifies to $S(qR_g)=1$ and $S(qR_g)=(qR_g)^{-D_f}$, respectively [2]. In these two limiting cases, the aggregate scattering cross-section $\langle C^a_{sca,RDG}\rangle$ is proportional to N_s^2 and N_s, respectively. In the first case, the scattered waves are in phase and their amplitudes add constructively [2]. In the second case, the phases are random and the waves add randomly [2].

Finally, the unpolarized scattering phase function $F_{11,RDG}(\Theta)$ of the aggregate predicted by the RDG approximation is expressed as [35]

$$F_{11,RDG}(\Theta) = \frac{1}{2}\frac{\langle C^a_{sca,vv,RDG}\rangle}{\langle C^a_{sca,RDG}\rangle}\left(1+\cos^2\Theta\right) \tag{12}$$

where the vertically polarized scattering cross-section of the aggregate for vertically polarized incident radiation, denoted by $\langle C^a_{sca,vv,RDG}\rangle$, is defined as [35]

$$\langle C^a_{sca,vv,RDG}\rangle = N_s \langle C_{sca,vv,R}\rangle S(qR_g). \tag{13}$$

The asymmetry factor g_{RDG} of the aggregate can also be estimated from the scattering phase function $F_{11,RDG}(\Theta)$ using Eq. (5).

The validity of the RDG approximation has been investigated in numerous studies. Farias et al. [35] compared absorption and scattering cross-sections predicted by the RDG approximation with those estimated by volume integral formulation of Maxwell's equations [31]. The authors examined randomly oriented aggregates of fractal dimensions D_f between 1.0 and 3.0 with monomer size parameter χ_s ranging from 0.01 to 1.0, and $|m-1|$ between 0.1 and 2.0. The RDG approximation predicted the scattering cross-section of aggregates consisting of 16–256 monodisperse monomers within 10% of those predicted by the volume integral method for size parameter $\chi_s < 0.3$. However, the accuracy of predictions of both absorption and scattering cross-sections by the RDG approximation deteriorated with increasing size parameter χ_s [35]. Wang and Sorensen [47] experimentally validated the RDG approximation by comparing the measured scattering cross-sections at 488 nm of aggregates with fractal dimension D_f of 1.75, composed of monodisperse monomers 20 nm in diameter made of SiO_2 ($m=1.46$) or TiO_2 ($m=2.61$). Note that at this wavelength, absorption by the aggregates could be ignored. On the other hand, Bushell [48] measured the scattering intensity of aggregates of latex particles 4.9 μm in diameter using a forward light scattering photometer. The author found poor agreement between experimental measurements and predictions by the RDG approximation and instead recommended using the T-matrix method.

2.4. Numerical predictions of aggregate radiation characteristics

The superposition T-matrix method [29], the generalized multiparticle-Mie theory [30], and the volume integral method [31] provide numerical solutions to Maxwell's equations for aggregates with arbitrary fractal dimension and number of monomers. For example, the superposition T-matrix method estimates the total scattered electromagnetic field at any given location by summing the contribution from each monomer [29].

Liu et al. [49] used the generalized multiparticle-Mie theory to predict the absorption and scattering cross-sections of soot aggregates featuring fractal dimension D_f of 1.4, 1.78, or 2.1 and a fractal prefactor k_f of 2.3. The aggregates were composed of up to 800 monodisperse monomers with size parameter $\chi_s=0.18$ and relative complex index of refraction $m=1.6+i0.6$. They demonstrated that both aggregate absorption and scattering cross-sections normalized, respectively, by the product of the number of monomers in the aggregate and the absorption or scattering cross-sections of a single monomer, i.e., $\langle C^a_{abs}\rangle/N_s\langle C_{abs}\rangle$ or $\langle C^a_{sca}\rangle/N_s\langle C_{sca}\rangle$, increased as a function of N_s for aggregates of all fractal dimensions and number of monomers considered. The authors attributed both of these observations to multiple scattering. In a similar study, Liu et al. [50] demonstrated that the normalized absorption cross-section per monomer $\langle C^a_{abs}\rangle/N_s\langle C_{abs}\rangle$ decreased as a function of N_s for soot aggregates featuring a fractal dimension D_f of 1.78 and a fractal prefactor k_f of 1.3 or 2.3. The aggregates were composed of 20 or more monomers of size parameter χ_s of 0.354 and relative complex index of refraction $m=1.6+i0.6$. The decrease

in $\langle C^a_{abs}\rangle/N_s\langle C_{abs}\rangle$ was attributed to the fact that outer particles of the aggregates shielded the inner ones from the incident radiation. Moreover, the normalized scattering cross-section per monomer $\langle C^a_{sca}\rangle/N_s\langle C_{sca}\rangle$ increased as a function of N_s due to multiple scattering [50].

Iskander et al. [31] developed a method for predicting the absorption and scattering cross-sections and the scattering matrix elements of aggregates by solving the volume integral formulation of Maxwell's equations [44]. This method is also known as the discrete dipole approximation and has been reviewed by Yukin and Hoekstra [51]. Manickavasagam and Mengüç [52] used this method to predict the scattering matrix elements of randomly oriented soot aggregates with fractal dimension D_f and prefactor k_f equal to 1.7 and 5.8, respectively. The numerically generated aggregates contained up to 150 monodisperse monomers of radius 20, 40, or 60 nm and relative complex index of refraction equal to $1.8+i0.5$. The authors concluded that the scattering phase function $F_{11}(\Theta)$ could not be used to identify either the number N_s of monomers in an aggregate or the monomer radius a. However, they demonstrated that spectral and angular variations in the scattering matrix element ratio $F_{21}(\Theta)/F_{11}(\Theta)$ could be used to determine both N_s and a. By contrast, the angular peaks in the scattering matrix element ratio $F_{34}(\Theta)/F_{11}(\Theta)$ depended on the monomer radius a but not on the number of monomers N_s [52]. The authors hypothesized that these peaks could be used to identify the monomer radius.

These different methods have been used to predict the radiation characteristics of soot aggregates [1,3,40,49,52–55], snow [56], comets [4], and cosmic dust aggregates [4]. In these applications, the monomers are relatively small compared with the radiation wavelength such that $\chi_s \ll 1$. However, as the size and number of monomers in the aggregate increase, the computational time and resources necessary to predict the radiation characteristics of the aggregates, using any of these numerical methods, increases sharply [4,34].

2.5. Equivalent particle approximations

Latimer [57] approximated fractal aggregates as coated spheres with equivalent volume and collision diameter. The coating had a relative complex index of refraction identical to that of the monomers constituting the aggregate while the core had the same index of refraction as the surrounding medium. The ratio of the total volume of monomers and the volume of the smallest sphere enclosing the aggregate was denoted by F and derived from fractal theory as [57]

$$F = N_s^{(1-3/D_f)}. \tag{14}$$

This expression assumed that the aggregate formed a solid sphere when D_f was equal to 3.0. The resulting equivalent coated sphere had an outer diameter equal to the collision diameter of the aggregates. The inner $a_{i,L}$ and outer $a_{o,L}$ radii of the coated sphere were given by [57]

$$a_{i,L} = N_s^{1/3} a\left(1-\frac{1}{F^{1/3}}\right) \quad \text{and} \quad a_{o,L} = \left(\frac{a^3 N_s}{F}\right)^{1/3} \tag{15}$$

Latimer [57] rationalized his approach by hypothesizing that the morphological features of aggregates composed of large monomers ($\chi_s \gg 1$) did not have any effect on their radiation characteristics due to their random orientation. The author experimentally measured the scattered intensity of a 474 nm laser beam incident by aqueous suspensions of aggregates consisting of latex microspheres, with diameter ranging from 0.26 to 2.05 μm ($1.7 \le \chi_s \le 13.6$). Theoretical predictions of the scattered laser intensity fell within 15% of experimental measurements for scattering angles 0–10° for all aggregate suspensions. However, the relative error reached up to 80% for scattering angles greater than 90° [57]. Therefore, a more rigorous validation of Latimer's method of approximating radiation characteristics of aggregates as volume and collision diameter equivalent coated spheres must be performed.

Finally, Morel and co-workers [58,59] demonstrated that the radiation characteristics of spheroidal microorganisms with an aspect ratio smaller than 1.5 can be treated as those of spheres. In addition, Lee et al. [60] also established that randomly oriented spheroidal microalgae cells, with an average aspect ratio of 1.333, could be treated as spheres over the photosynthetically active radiation (PAR) region.

The present study aims to find a simplified method for predicting the radiation characteristics of fractal aggregates, in particular, those with a large number of monomers of large size parameter χ_s, beyond the range of validity of the RDG approximation. Absorption and scattering cross-sections as well as scattering matrix element ratios of fractal aggregates with fractal dimension ranging from 2.0 to 3.0 were computed using the superposition T-matrix method. These results were compared with predictions made by (1) the RDG approximation, (2) Latimer's coated sphere approximation, and (3) the volume and average projected area equivalent coated sphere approximation. Fractal aggregates composed of up to 1000 monodisperse or polydisperse spherical monomers featuring size parameter ranging from 0.01 to 20 were considered.

3. Methods

3.1. Fractal aggregate generation

First, fractal aggregates were generated using the particle cluster aggregation program validated and released by Mroczka and co-workers [40,41,61]. All monomers in the aggregate were in contact with each other but did not overlap. The fractal dimension was taken as D_f=2.25 corresponding approximately to that of phytoplankton, as previously mentioned in Section 2.1 [8]. The fractal prefactor k_f was taken as 1.59 as prescribed by Sorensen [2] and Mroczka et al. [40]. The aggregates generated consisted of 2–1000 monomers featuring size parameter χ_s ranging from 0.01 to 20. In addition, ordered aggregates featuring integer fractal dimension D_f equal to 1.0, 2.0, and 3.0 were generated and corresponded to linear chain, square packing, and simple cubic packing of sphere, respectively.

The total volume V_T of an arbitrary aggregate with polydisperse spherical monomers of radius $(a_j)_{1\le j\le N_s}$ can

be written as

$$V_T = \sum_{j=1}^{N_s} \frac{4\pi}{3} a_j^3 \tag{16}$$

The radius $a_{eq,V}$ of the volume equivalent sphere can be expressed as

$$a_{eq,V} = \left(\frac{3}{4\pi} V_T\right)^{1/3}. \tag{17}$$

The radius $\langle a \rangle$ of the volume-averaged monomer is given by

$$\langle a \rangle = \left(\frac{3}{4\pi} \frac{V_T}{N_s}\right)^{1/3}. \tag{18}$$

The corresponding volume-averaged size parameter can be defined as $\langle \chi_s \rangle = 2\pi \langle a \rangle \lambda^{-1}$. Alternatively, the average monomer size parameter $\overline{\chi}_s$ for aggregates composed of polydisperse monomers can be estimated as

$$\overline{\chi}_s = \frac{1}{N_s} \sum_{j=1}^{N_s} \frac{2\pi a_j}{\lambda}. \tag{19}$$

For aggregates consisting of monodisperse monomers, the volume averaged monomer radius $\langle a \rangle$ is equal to the monomer radius a and $\langle \chi_s \rangle = \overline{\chi}_s = \chi_s$.

The average projected area $\overline{A}_p$ of the aggregates was estimated numerically using the method discussed in detail by Heng et al. [62]. In brief, the aggregate's center of mass was fixed with respect to the observer and the aggregate was rotated through a large number of discrete orientations. Then, the orientation-averaged area projected onto a plane normal to the line of sight was calculated. Finally, the outer $a_{o,V+\overline{A}_p}$ and inner $a_{i,V+\overline{A}_p}$ radii of the volume and average projected area equivalent coated sphere can be expressed as

$$a_{o,V+\overline{A}_p} = \left(\frac{\overline{A}_p}{\pi}\right)^{1/2} \quad \text{and} \quad a_{i,V+\overline{A}_p} = \left(a_{o,V+\overline{A}_p}^3 - \frac{3}{4\pi} V_T\right)^{1/3} \tag{20}$$

This ensures that the volume of the coating and the projected area of the equivalent coated sphere were the same as the total volume V_T and the average projected area $\overline{A}_p$ of the aggregate.

3.2. Radiation characteristic predictions

First, the orientation averaged absorption $\langle C_{abs}^a \rangle$ and scattering $\langle C_{sca}^a \rangle$ cross-sections and scattering matrix elements of aggregates consisting of monodisperse and polydisperse spherical monomers were predicted using the superposition T-matrix method using the program developed by Mackowski and Mishchenko [29]. The medium surrounding the aggregates was non-absorbing and had an index of refraction equal to that of water in the visible part of the spectrum, i.e., $n_m = 1.33$. Unless stated otherwise, the monomers featured a complex index of refraction $m_p = 1.355 + i0.004$. This resulted in a relative complex index of refraction $m = m_p/n_m = 1.0165 + i0.003$ representative of various microalgae species [23,60]. The position of each monomer and their individual size parameter χ_s were prescribed while they were all assumed to have the same relative complex index of refraction m. Then, the orientation-averaged aggregate absorption $\langle Q_{abs}^a \rangle$ and scattering $\langle Q_{sca}^a \rangle$ efficiency factors were computed. Finally, the absorption $\langle C_{abs}^a \rangle$ and scattering $\langle C_{sca}^a \rangle$ cross-sections of the randomly oriented aggregates were estimated according to [29]

$$\langle C_{abs/sca}^a \rangle (N_s, \chi_s, m, D_f, k_f) = \langle Q_{abs/sca}^a \rangle (N_s, \chi_s, m, D_f, k_f) \pi a_{eq,V}^2 \tag{21}$$

where the volume equivalent sphere radius $a_{eq,V}$ is given by Eq. (17).

Moreover, the orientation-averaged absorption $\langle C_{abs,RDG}^a \rangle$ and scattering $\langle C_{sca,RDG}^a \rangle$ cross-sections and the scattering phase function $F_{11,RDG}(\Theta)$ of the aggregates were predicted by the RDG approximation using Eqs. (7), (9), and (12), respectively. For aggregates composed of polydisperse monomers, the monomer size parameter χ_s in Eqs. (8) and (10) was replaced by the volume-averaged size parameter $\langle \chi_s \rangle$.

The absorption and scattering cross-sections and the scattering matrix elements of the volume and average projected area equivalent coated spheres were predicted based on Lorenz–Mie theory using the program developed by Matzler [63]. First, their absorption and scattering efficiency factors were computed based on (i) the size parameters $\chi_{i,\overline{A}_p+V}$ and $\chi_{o,\overline{A}_p+V}$ associated with the inner $a_{i,V+\overline{A}_p}$ and outer $a_{o,V+\overline{A}_p}$ radii given by Eq. (20) and (ii) the relative complex index of refraction m. Then, the absorption $\langle C_{abs,V+\overline{A}_p} \rangle$ and scattering $\langle C_{sca,V+\overline{A}_p} \rangle$ cross-sections were estimated according to

$$\begin{aligned} &\langle C_{abs/sca,V+\overline{A}_p} \rangle (\chi_{i,\overline{A}_p+V}, \chi_{o,\overline{A}_p+V}, m) \\ &= \langle Q_{abs/sca,V+\overline{A}_p} \rangle (\chi_{i,\overline{A}_p+V}, \chi_{o,\overline{A}_p+V}, m) \pi a_{o,V+\overline{A}_p}^2 \end{aligned} \tag{22}$$

Similarly, the absorption $\langle C_{abs,L} \rangle$ and scattering $\langle C_{sca,L} \rangle$ cross-sections corresponding to Latimer's equivalent coated sphere were estimated using Eq. (22) by replacing the size parameters $\chi_{i,V+\overline{A}_p}$ and $\chi_{o,V+\overline{A}_p}$ with the size parameters $\chi_{i,L}$ and $\chi_{o,L}$ corresponding to the inner $a_{i,L}$ and outer $a_{o,L}$ radii given by Eq. (15).

Finally, the relative errors in the absorption and scattering cross-sections of the aggregates between predictions by the superposition T-matrix method and the RDG and the equivalent coated sphere approximations were estimated in order to identify the best approximation method.

4. Results

4.1. Average projected area

First, the average projected area $\overline{A}_p$ of aggregates composed of monodisperse monomers was computed using the code developed by Heng et al. [62]. The monomers had radius a equal to 1, 5, or 10 μm. The number of monomers per aggregates N_s ranged from 2 to 1000 while the fractal dimension D_f was taken as 1.0, 1.75, 2.0, 2.25, 2.5, or 3.0. In all cases, for aggregates of a given fractal dimension D_f and monomers number N_s, the ratio $\overline{A}_p/a^2$ was found to be constant. Fig. 2 plots the dimensionless ratio $\overline{A}_p/a^2$ as a function of the number of monomers N_s in the aggregate for different values of D_f. It indicates that $\overline{A}_p/a^2$ increased with the number of monomers N_s for all fractal dimensions

considered. Moreover, for aggregates with identical monomer number N_s and radius a, the average projected area increased with decreasing fractal dimension D_f. This was consistent with fractal theory which dictates that aggregates with larger fractal dimension feature a more compact structure [2]. Finally, the ratio $\overline{A}_p/a^2$ was fitted by the least squares method to a power-law in terms of N_s to yield

$$\frac{\overline{A}_p}{a^2} = \pi N_s^{\alpha} \tag{23}$$

where the exponent α was a function of fractal dimension D_f. The constant π was used to ensure the validity of Eq. (23) in the limiting case of a single sphere when $N_s=1$ and $\overline{A}_p = \pi a^2$. The power α was found to decrease monotonously from α_{max} of 0.92 for linear chains of spheres with $D_f=1.0$ to α_{min} of 0.73 for $D_f=3.0$. The inset of Fig. 2 shows the reduced variables $\alpha^* = (\alpha-\alpha_{min})/(\alpha_{max}-\alpha_{min})$ plotted versus $D_f^* = (D_f-1)/2$ whose least-squares fitting yielded the following correlation:

$$\alpha^* = (1+D_f^{*1.8})^{1/1.8} \tag{24}$$

For both power-law fits of Eqs. (23) and (24), the coefficient of determination R^2 was larger than 0.99. The average projected area estimated by Eqs. (23) and (24) was used to predict the outer radius $a_{o,V+\overline{A}_p}$ of the equivalent coated sphere according to Eq. (20).

4.2. Absorption and scattering cross-sections

4.2.1. Effect of aggregate fractal dimension

Fig. 3a, b, and c shows the absorption $\langle C_{abs}^a \rangle$ and scattering $\langle C_{sca}^a \rangle$ cross-sections of randomly oriented aggregates as functions of the number of monodisperse monomers N_s ranging from 2 to 1000 for fractal dimension D_f equal to 2.0, 2.25, and 3.0, respectively. Each monomer featured radius a equal to 1 μm and size parameter χ_s equal to 1, while its relative complex index of refraction m was equal to $1.0165+i0.003$. Note that the monomer size parameter χ_s of 1 was chosen because it falls outside the Rayleigh scattering regime and it was the largest size parameter for which computation of aggregates containing as many as 1000 monomers was possible. Fig. 3a–c also compares the absorption and scattering cross-sections predicted by the superposition T-matrix method with those estimated by (i) the RDG approximation, (ii) Latimer's coated sphere approximation, and (iii) the equivalent volume and average projected area coated sphere approximation. In all cases, the absorption cross-section $\langle C_{abs}^a \rangle$ was proportional to the number of monomers N_s. In fact, $\langle C_{abs}^a \rangle$ was independent of the fractal prefactor and dimension k_f and D_f. In addition, for all values of N_s and D_f investigated, the three different approximations considered predicted aggregate absorption cross-section $\langle C_{abs}^a \rangle$ within less than 1% of predictions by the superposition T-matrix method. This can be attributed to the fact that, for aggregates composed of monomers with relatively small absorption index k_s (i.e., optically soft), absorption is a volumetric phenomenon. For all approximations, the volume of material interacting with the incident electromagnetic wave was identical to the total volume V_T of the aggregates. Thus, for aggregates composed of monodisperse monomers, Eq. (7) can also be expressed as $\langle C_{abs}^a \rangle = V_T/V_s \langle C_{abs} \rangle$, where V_s corresponds to the volume of a single monomer. In other words, the absorption cross-section $\langle C_{abs}^a \rangle$ of any randomly oriented fractal aggregate considered was proportional to its total volume V_T. The same conclusion was reached for linear chains of spheres [34] and for bispheres, quadspheres, and rings of spheres [62] made of optically soft monomers.

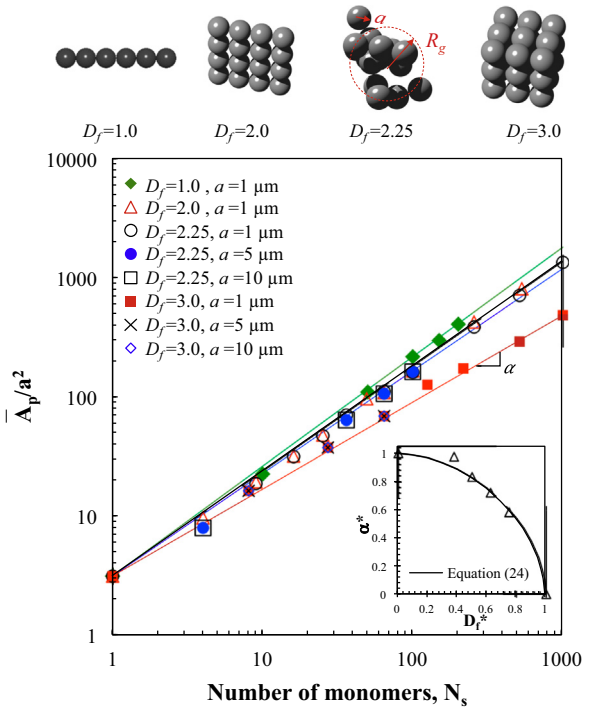

Fig. 2. The ratio $\overline{A}_p/a^2$ as a function of number N_s of monodisperse monomers in an aggregate for fractal dimension D_f equal to 1.0, 1.75, 2.0, 2.25, 2.5, and 3.0 and monomer radii a equal to 1, 5, and 10 μm.

Similarly, the scattering cross-section $\langle C_{sca}^a \rangle$ increased as a function of number of monomers N_s present in the aggregates. Here, $\langle C_{sca}^a \rangle$ was proportional to N_s^p where the power p was equal to 1.27, 1.30, and 1.40 for aggregates with fractal dimension D_f of 2.0, 2.25, and 3.0, respectively. Thus, unlike for $\langle C_{abs}^a \rangle$, the scattering cross-section of the aggregate was larger than the sum of the scattering cross-sections of each monomer (i.e., $p>1$) due to multiple scattering. In fact, for a given number of monomers N_s and a given total volume V_T, the aggregates with larger fractal dimension D_f featured larger scattering cross-sections $\langle C_{sca}^a \rangle$. This was due to the fact that increasing the fractal dimension D_f resulted in a smaller average projected area (Fig. 2) and a more compact structure more prone to multiple scattering [53]. The relative error between scattering cross-section $\langle C_{sca}^a \rangle$ predicted by the T-matrix method and that estimated by the RDG approximation was smaller than 15% for aggregates containing fewer than 100 monomers for any fractal dimension D_f considered. However, it reached up to 40% for aggregates containing 100 or more monomers. On the other hand, the relative error in the scattering cross-section predicted by Latimer's coated sphere approximation was smaller than 18% for fractal dimension D_f equal to 2.25 corresponding to the value of

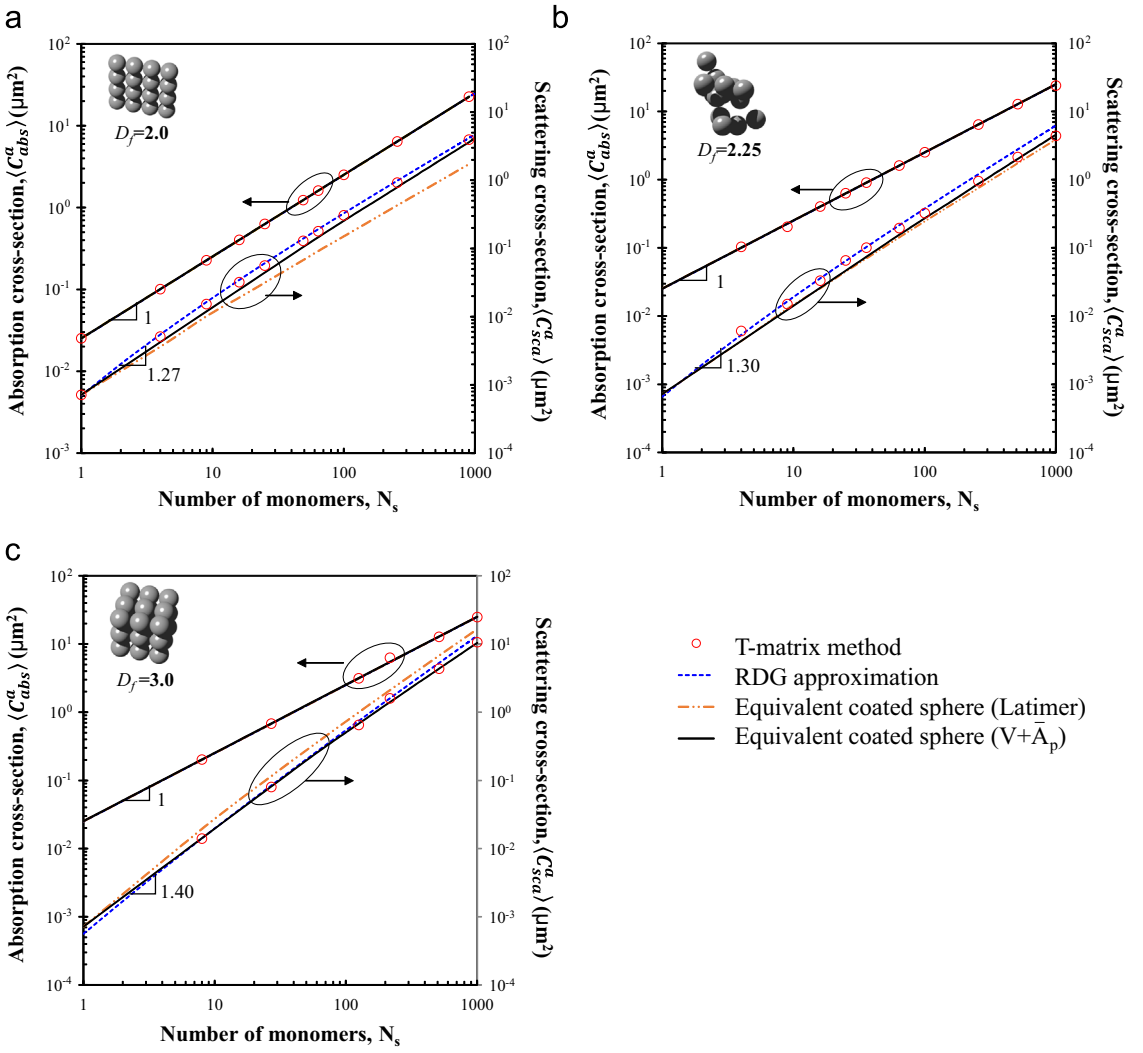

Fig. 3. Absorption $\langle C^a_{abs}\rangle$ and scattering $\langle C^a_{sca}\rangle$ cross sections as functions of monomer number N_s in randomly oriented aggregates with fractal dimension D_f of (a) 2.0, (b) 2.25, and (c) 3.0 predicted using the superposition T-matrix method, the RDG approximation, Latimer's [57] coated sphere approximation, and the volume and average projected area equivalent coated sphere approximation. The aggregates were composed of monodisperse monomers featuring size parameter $\chi_s=1$ and $m=1.0165+i0.003$.

D_f validated by Latimer [57]. Note that Latimer's choice to reduce the monomer number distribution of a large number of aggregates to only five discrete bins was arbitrary and may have introduced larger errors in the theoretical predictions of the scattering cross-section known to be very sensitive to the number of monomers N_s [2,44]. Indeed, the relative error in the scattering cross-section predicted by Latimer's coated sphere approximation reached up to 47% for fractal dimensions D_f of 2.0 and 3.0. Due to the relatively large discrepancies between predictions by the T-matrix method and by Latimer's approximation [57], the latter was omitted in the remainder of this study. By contrast, the scattering cross-section of the volume and average projected area equivalent coated sphere fell within 7.5% of that predicted by the T-matrix method for all values of N_s and D_f considered. Note that predictions of the integral radiation characteristics for the volume-equivalent or surface-area-equivalent homogeneous spheres were not as accurate as those for the volume and average projected area equivalent coated sphere.

4.2.2. *Effect of size parameter*

Fig. 4a–d shows the absorption $\langle C^a_{abs}\rangle$ and scattering $\langle C^a_{sca}\rangle$ cross-sections of randomly oriented aggregates of monodisperse monomers with fractal dimension D_f=2.25 as a function of monomer number N_s for size parameter χ_s equal to 0.01, 0.1, 0.5, 5, 10, and 20. They compare the superposition T-matrix predictions with those of the RDG approximation and for the volume and average projected area equivalent coated sphere. They indicate that both absorption $\langle C^a_{abs}\rangle$ and scattering $\langle C^a_{sca}\rangle$ cross-sections increased with increasing number of monomers N_s and size parameter χ_s. More specifically, Fig. 4a and c establishes that the aggregate absorption cross-section $\langle C^a_{abs}\rangle$ was linearly proportional to the number of monomers N_s for all size parameters considered. On the other hand, Fig. 4b reveals that the aggregate

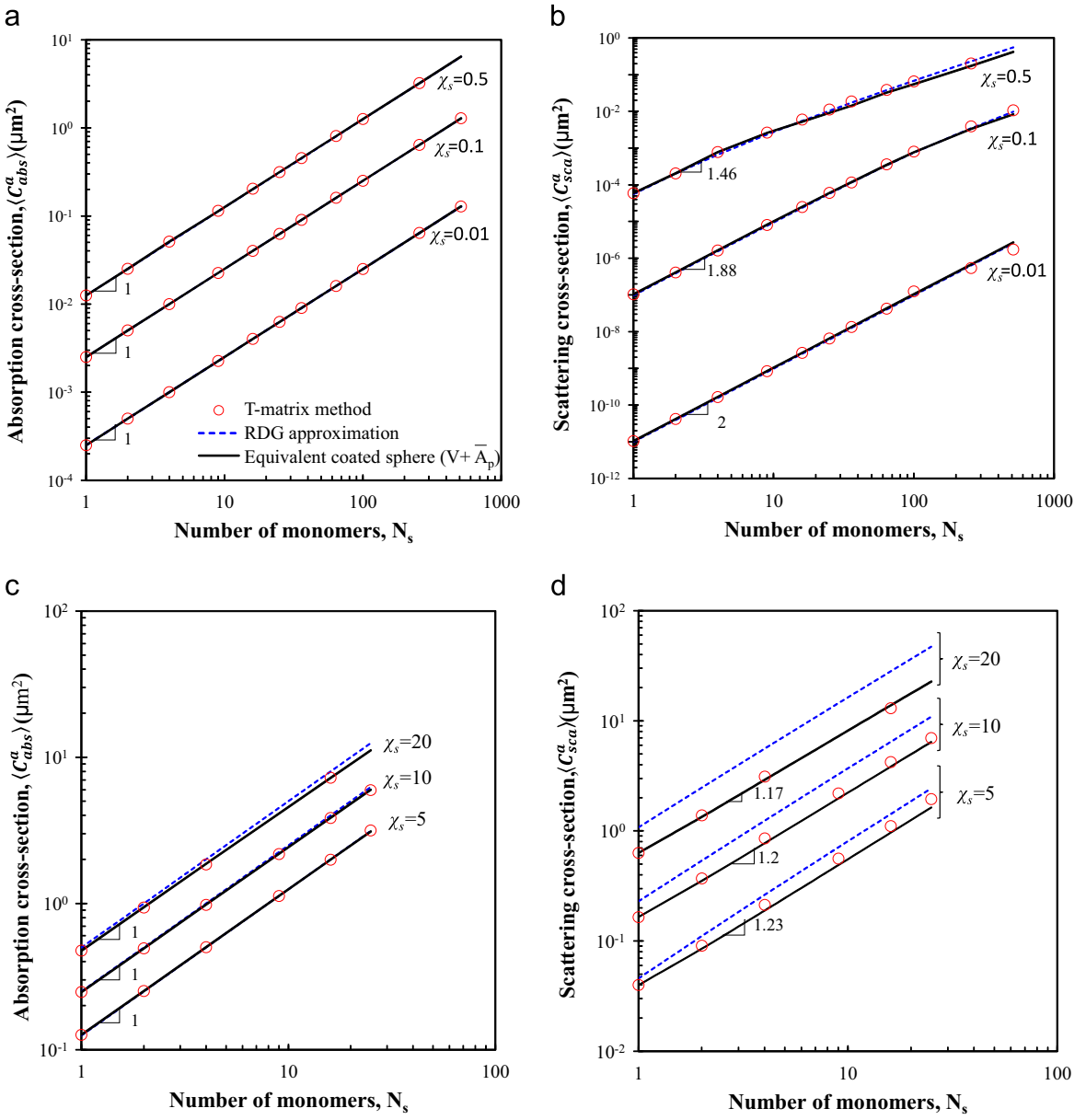

Fig. 4. (a, c) Absorption $\langle C^a_{abs}\rangle$ and (b, d) scattering $\langle C^a_{sca}\rangle$ cross-sections as functions of monomer number N_s in randomly oriented aggregates with fractal dimension D_f=2.25 and composed of monomers with $m = 1.0165 + i0.003$ and size parameter χ_s ranging from 0.01 to 20 predicted using (i) the superposition T-matrix method, (ii) the RDG approximation, and (iii) the volume and average projected area equivalent coated sphere approximation.

scattering cross-section $\langle C^a_{sca}\rangle$ was proportional to N_s^2 for aggregates composed of monomers of size parameter $\chi_s = 0.01$. It is interesting to note that, in the limiting case of for small size parameter χ_s and small aggregates such that $\chi_s \ll 1$ and $qR_g \ll 1$, the RDG approximation predicts that $\langle C^a_{sca}\rangle$ is proportional to N_s^2. Fig. 4b and d indicates that $\langle C^a_{sca}\rangle$ was proportional to N_s^p with a power-law exponent p that monotonously decreased from 2 to 1.17 as the monomer size parameter χ_s increased from 0.01 to 20. In fact, in the limiting case of large size parameter χ_s and large aggregates, i.e., $\chi_s \ll 1$ and $qR_g \ll 1$, the RDG approximation predicts that $\langle C^a_{sca}\rangle$ is linearly proportional to N_s (i.e., $p=1$), as previously mentioned in Section 2.3.

The absorption cross-section predicted by the RDG approximation and the volume and average projected area equivalent coated sphere fell within 5% of the T-matrix predictions for all values of N_s and χ_s considered. In addition, the relative error in scattering cross-section predictions by the RDG approximation was smaller than 8% for size parameter χ_s smaller than 0.5. This confirms and expands on the findings by Farias et al. [35] and by Wang and Sorensen [47] as previously discussed in Section 2.3. However, it reached 29%, 56%, and 117% for size parameters χ_s of 5, 10, and 20, respectively. This excessively large relative error in scattering cross-section renders the RDG approximation unsuitable for predicting the radiation

characteristics of aggregates composed of monomers of size parameter larger than 1, as previously reported in the literature [35,38,47,48]. By contrast, the scattering cross-section of the volume and average projected area equivalent coated sphere fell within 10% of the predictions by the T-matrix method for all values of N_s and χ_s considered. In other words, the volume and average projected area equivalent coated sphere was able to capture the multiple scattering effects on the integral radiation characteristics.

Moreover, note that the maximum number of monomers per aggregate that could be simulated decreased with increasing monomer size parameter χ_s. For example, a converged solution for aggregates of 25 monomers of size parameter $\chi_s = 20$ could not be obtained using the superposition T-matrix program despite the use of a relatively large computer cluster. Moreover, for a fractal aggregate containing 25 monomers of size parameter $\chi_s = 10$, the superposition T-matrix code yielded a converged solution after 25 h running in parallel on 135 CPUs. Alternatively, predictions of the radiation characteristics and scattering matrix elements of the corresponding volume and average projected area equivalent coated spheres were obtained in 3.6 ms using a computer with a single core CPU. Thus, this approximation could provide an invaluable tool for estimating the radiation characteristics of randomly oriented aggregates with reasonable accuracy, particularly for aggregates with a large number of large monomers. For example, it could be used in inverse problems aiming to infer the aggregate morphology and/or the monomer complex index of refraction from experimental measurements [36,60,64,65]. It could also be used when the superposition T-matrix method fails to converge or if the necessary computing resources are not available. This is particularly interesting for microalgae colonies consisting of cells 4–12 μm in diameter (Fig. 1e and f) and featuring size parameter χ_s ranging between 18 and 95 over the PAR region (λ=400–700 nm). For such suspensions, the volume and average projected area equivalent coated sphere approximation can predict, rapidly and sufficiently accurately, the absorption and scattering cross-sections as well as the asymmetry factor g or the backward scattering fraction b needed to perform radiation transfer analysis in PBRs [25,66,67].

4.2.3. Effect of polydispersity

To investigate the effects of monomer polydispersity on the aggregates' absorption and scattering cross-sections, aggregates composed of 256, 512, and 1000 polydisperse monomers were generated with a Gaussian radius distribution with the same mean radius of 1 μm and standard deviation of 10% or 25%. Table 1 reports the mean $\overline{\chi}_s$ and volume-averaged $\langle\chi_s\rangle$ size parameters and the average projected area of the aggregates generated. It also compares predictions of the corresponding absorption $\langle C^a_{abs}\rangle$ and scattering $\langle C^a_{sca}\rangle$ cross-sections by the superposition T-matrix method with those made by the RDG and the volume and average projected area equivalent coated sphere approximations. In all cases, the monomer mean size parameter $\overline{\chi}_s$ was equal to 1 and the fractal dimension D_f was equal to 2.25. However, the total volume V_T and the volume-averaged size parameter $\langle\chi_s\rangle$ of the aggregates with polydisperse monomers were larger than those with monodisperse monomers for the same number of monomers N_s. On the other hand, the average projected area $\overline{A}_p$ of the aggregates increased only slightly with polydispersity of the monomers. Overall, the ratio $\overline{A}_p/V_T$ of the average projected area to the total volume was smaller for aggregates with polydisperse monomers than with monodisperse monomers having the same monomer number and mean radius. In other words, aggregates with polydisperse monomers were more compact that those with monodisperse monomers.

Moreover, for all cases considered, aggregates composed of polydisperse monomers featured larger absorption and scattering cross-sections than those composed of the same number of monodisperse monomers N_s. The larger absorption cross-section was due to the fact that the total volume of the aggregates V_T increased with increasing monomer polydispersity, as reported in Table 1. On the other hand, the increase in aggregate scattering cross-section $\langle C^a_{sca}\rangle$ could be attributed to the fact that the aggregates were more compact and therefore more prone to multiple scattering. These results were consistent with the conclusion reached for aggregates with monodisperse monomers and different fractal dimensions (Fig. 3).

Finally, the absorption cross-sections of the randomly oriented aggregates with polydisperse monomers predicted

Table 1
Absorption $\langle C^a_{abs}\rangle$ and scattering $\langle C^a_{sca}\rangle$ cross-sections of randomly oriented aggregates of fractal dimension D_f of 2.25 composed of monomers with a Gaussian radius distribution and standard deviations of 0%, 10%, and 25%. The aggregates were composed of 256, 512, and 1000 monomers with mean size parameter $\overline{\chi}_s$=1 and relative complex index of refraction $m = 1.0165 + i0.003$.

				T-matrix				Rayleigh–Debye–Gans approximation				Equivalent coated sphere			
N_s	χ_s stdev (%)	$\overline{\chi}_s$	$\langle\chi_s\rangle$	V_T (μm^3)	$\overline{A}_p$ (μm^2)	$\langle C^a_{abs}\rangle$ (μm^2)	$\langle C^a_{sca}\rangle$ (μm^2)	$\langle C^a_{abs,RDG}\rangle$ (μm^2)	Error (%)	$\langle C^a_{sca,RDG}\rangle$ (μm^2)	Error (%)	$\langle C^a_{abs,V+\overline{A}_p}\rangle$ (μm^2)	Error (%)	$\langle C^a_{sca,V+\overline{A}_p}\rangle$ (μm^2)	Error (%)
256	0	1.0	1.00	1072	386	6.44	0.96	6.4	0.62	1.14	−19	6.4	0.01	0.83	14
256	10	1.0	1.01	1093	389	6.63	1.01	6.6	0.60	1.18	−17	6.6	0.3	0.91	10
256	25	1.0	1.08	1335	424	8.03	1.42	8.0	0.75	1.55	−9.2	8.0	0	1.2	14
512	0	1.0	1.00	2145	707	12.9	2.18	12.8	0.78	2.64	−21	12.9	0.2	2.0	10
512	10	1.0	1.00	2145	711	12.8	2.14	12.7	0.78	2.61	−22	12.8	0	2.0	8.4
512	25	1.0	1.06	2567	768	15.4	2.89	15.3	0.65	3.4	−18	15.4	0	2.7	8.0
1000	0	1.0	1.00	4189	1341	24.1	4.39	25.0	−3.4	5.9	−34	25.1	4.0	4.4	−0.5
1000	10	1.0	1.02	4376	1365	26.0	4.78	25.8	0.77	6.2	−29	26.0	0	4.5	5.7
1000	25	1.0	1.07	5059	1408	30.3	6.2	30.2	0.33	7.7	−24	30.3	0	5.9	5.7

by both the RDG and the volume and average projected area equivalent coated sphere approximations fell within 4% of the predictions by the superposition T-matrix method. However, the associated scattering cross-section predicted by the RDG approximation suffered from a relative error of up to 29% for aggregates containing 1000 monomers. By contrast, the relative error in the scattering cross-section predicted for the volume and average projected area equivalent coated sphere was less than 14% for all aggregates considered. This confirms the validity of volume and average projected area equivalent coated sphere approximation in predicting the absorption and scattering cross-sections of randomly oriented fractal aggregates consisting of either monodisperse or polydisperse optically soft monomers.

4.2.4. *Effect of the relative complex index of refraction*

Fig. 5a and b plots the absorption and scattering cross-sections of randomly oriented aggregates normalized by the product of the monomer number N_s and the absorption and scattering cross-sections of a single spherical monomer $\langle C^a_{abs}\rangle/N_s\langle C_{abs}\rangle$ and $\langle C^a_{sca}\rangle/N_s\langle C_{sca}\rangle$ as a function of N_s, respectively. All aggregates featured a fractal dimension D_f of 2.25, monodisperse monomers with size parameter $\chi_s = 1$, and relative refractive index $n=1.0165$. The relative absorption index k was taken as 0.003, 0.03, 0.07, or 0.5. A ratio $\langle C^a_{abs}\rangle/N_s\langle C_{abs}\rangle$ or $\langle C^a_{sca}\rangle/N_s\langle C_{sca}\rangle$ independent of N_s and equal to unity would indicate that the absorption or scattering cross-section of the aggregate is the sum of absorption or scattering cross-sections of its constituent monomers. In fact, the normalized absorption cross-section per monomer $\langle C^a_{abs}\rangle/N_s\langle C_{abs}\rangle$ remained constant and equal to unity for aggregates with relative absorption index $k=0.003$. This was consistent with the RDG approximation expression for $\langle C^a_{abs,RDG}\rangle$ given by Eq. (7) in Section 2.3. However, for relative absorption index larger than 0.003, the normalized absorption cross-section was smaller than 1.0 and decreased with increasing values of N_s and k. Similar observations were made by Liu et al. [50] for soot aggregates composed of monomers with absorption index k of 0.6 and size parameter χ_s of 0.354, as previously discussed in Section 2.4. This can be attributed to the shading of the monomers located inside the aggregates by those located on the outside. This phenomenon was particularly important for aggregates composed of large, numerous, and/or strongly absorbing monomers. In addition, the scattering cross-section of aggregates composed of strongly absorbing monomers was much larger than for those composed of weakly absorbing monomers. These relatively large absorption and scattering cross-sections caused the incident electromagnetic wave to be fully attenuated before it can reach the inner monomers. For such aggregates, the absorption cross-section did not depend linearly on the material volume interacting with the incident radiation, unlike what has been observed for optically soft particles aggregates [49,50]. Instead, when the penetration depth was smaller than the monomer size, absorption became a surface phenomenon.

Moreover, the normalized scattering cross-section per monomer represented by $\langle C^a_{sca}\rangle/N_s\langle C_{sca}\rangle$, increased with increasing N_s and was larger than 1.0 for all four complex indices of refraction considered. In other words, the scattering cross-section of an aggregate was larger than the sum of the scattering cross-sections of its constitutive monomers. This can be attributed to multiple scattering as previously discussed. However, the latter was less significant for aggregates composed of strongly absorbing monomers due to the attenuation of the electromagnetic wave which could not emerge from the aggregate. Note that Mishchenko [68] presented the equality $\langle C^a_{ext}\rangle = N_s\langle C_{ext}\rangle$ as a necessary condition for single scattering to prevail in multi-particle aggregates. Moreover, the RDG approximation predictions of $\langle C^a_{abs}\rangle/N_s\langle C_{abs}\rangle$ and $\langle C^a_{sca}\rangle/N_s\langle C_{sca}\rangle$ as a function of N_s were independent of the relative absorption index k. This resulted in very large discrepancies with predictions by the superposition T-matrix method. On the

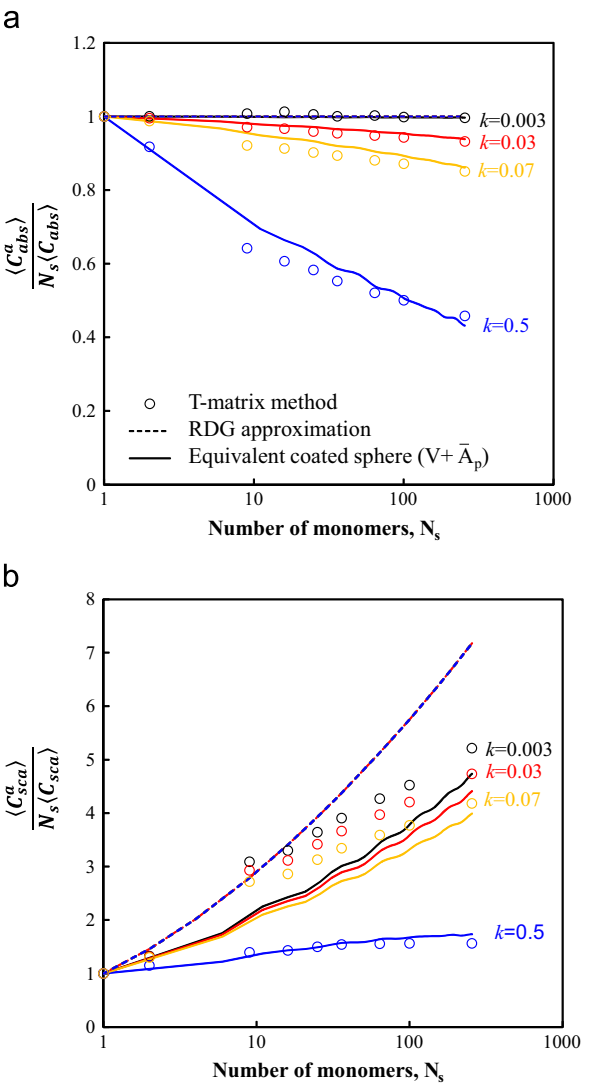

Fig. 5. Normalized (a) absorption $\langle C^a_{abs}\rangle/N_s\langle C_{abs}\rangle$ and (b) scattering $\langle C^a_{sca}\rangle/N_s\langle C_{sca}\rangle$ cross-sections as a function of N_s predicted by the superposition T-matrix method, the RDG approximation, and the volume and average projected area equivalent coated sphere approximation for different values of relative absorption index k. All aggregates had fractal dimension $D_f=2.25$, monomer size parameter $\chi_s=1$, and relative refraction index $n=1.0165$.

other hand, the volume and average projected area equivalent coated sphere predictions featured a relative error in the absorption and scattering cross-sections of less than 8% and 29%, respectively, compared with the T-matrix method for all values of N_s and k considered. Moreover, the relative error between predictions by the coated sphere approximation and by the T-matrix method decreased with increasing monomer absorption index. Indeed, the maximum relative error in the scattering cross-section was 29% and 11% for aggregates composed of monomers with relative complex index of refraction m equal to $1.0165+i0.003$ and $1.0165+i0.5$, respectively. This was in contrast to the relative error between the RDG approximation and the superposition T-matrix method predictions which increased with monomer absorption index. In fact, the scattering cross-sections estimated by the RDG approximation differed by more than 50% from those by the T-matrix method for aggregates composed of more than $N_s=100$ monomers with size parameter $\chi_s=1$ and relative absorption index k larger than 0.03. These results establish that the volume and average projected area equivalent coated sphere approximation could not only capture the effects of multiple scattering but also of shading among monomers.

Finally, these results indicate that the formation of colonies of microalgae in PBRs results in reduced absorption cross-section per cell and increased scattering cross-section per cell. Therefore, light transfer in microalgae suspensions will be strongly affected by colony formation.

4.3. Scattering phase function

Fig. 6a–f shows the scattering phase function $F_{11}(\Theta)$ of randomly oriented aggregates of fractal dimension D_f of 2.25 consisting of monomers of size parameter χ_s of 1 and 5 for a number of monomers N_s ranging from 9 to 100. They compare predictions by the superposition T-matrix method with those of (i) the RDG approximation, (ii) the volume and average projected area equivalent coated sphere approximation, and (iii) the Henyey–Greenstein phase function given by Eq. (6) using the asymmetry factor g corresponding to the phase function of the equivalent coated sphere.

First, scattering by randomly oriented aggregates was increasingly in the forward direction as the size parameter χ_s and/or the number of monomers N_s in the aggregate increased. Fig. 6a–c, corresponding to $\chi_s=1$, confirms the conclusions reached by Manickavasagam and Mengüç [52] (Section 2.4) that measurements of aggregate scattering phase function alone could not be used to identify the monomer size parameter χ_s or their number N_s for size parameter χ_s between 0.5 and 1.5. Indeed, these three aggregates did not feature any distinguishing characteristics that could be used to determine either χ_s or N_s. On the other hand, aggregates composed of monomers of size parameter $\chi_s=5$ featured scattering phase functions $F_{11}(\Theta)$ with two distinct resonance peaks at scattering angles Θ of 55° and 100°. These angles depended only on the monomer size parameter χ_s. However, the magnitude of these resonance peaks correlated to the number of monomer in the aggregate N_s. Therefore, these two unique features of the scattering phase function could be used to determine the monomer's size parameter χ_s and number N_s in aggregates composed of relatively large monomers.

Moreover, the approximate methods predicted similar phase functions for the aggregates composed of monomers of size parameter χ_s of 1. However, the equivalent coated sphere scattering phase function featured several resonance peaks at various scattering angles Θ. These peaks did not correspond to those observed in the phase function predicted by the T-matrix method. The number and magnitude of these resonance peaks increased with increasing monomer number N_s and size parameter χ_s. These resonance peaks are characteristic of coated spheres [69] and were due to internal reflection within the coating which acted as a waveguide.

Another indicator of multiple scattering is the aggregate scattering phase function at $\Theta=0°$. Indeed, single scattering by the aggregates requires that $F_{11}(0°)=N_sF_{11,s}(0°)$, where $F_{11,s}$ is the scattering phase function of a single sphere [68]. Here, the values of $F_{11}(0°)$ of the aggregates composed of 9 and 36 monomers of size parameter $\chi_s=1$ and relative complex index of refraction $m=1.0165+i0.003$ was equal to 19.9 and 79.6, respectively. On the other hand, $F_{11,s}(0°)$ for a single monomer of the same size parameter was equal to 2.21. Similarly, $F_{11}(0°)$ was 244 and 309 for aggregates composed of 16 and 25 monomers of size parameter 5, respectively. The corresponding $F_{11,s}(0°)$ was equal to 24.7. This further establishes the presence of multiple scattering in the aggregates considered in Fig. 6.

The inset tables in Fig. 6a–f report the asymmetry factor g corresponding to the scattering phase function predicted by the T-matrix method, the RDG approximation, and the volume and average projected area equivalent coated sphere approximation. They indicate that the asymmetry factor g increased from 0.62 for $\chi_s=1$ and $N_s=9$ to 0.96 for $\chi_s=5$ and $N_s=25$. The relative error in the asymmetry factor g predicted by the RDG approximation reached 10% compared with the T-matrix method predictions for $\chi_s=5$ and $N_s=25$. However, it was smaller than 5% for the volume and average projected area equivalent coated sphere for all values of χ_s and N_s considered. The asymmetry factor can be used in various approximate expressions of the scattering phase function including the transport approximation [70] and the HG approximate phase function. In fact, the latter gave reasonable predictions of $F_{11}(\Theta)$ of the aggregates for $\chi_s=1$ using the asymmetry factor corresponding to the equivalent coated sphere (Fig. 6a–c). Note that large errors were observed for aggregates with larger monomers ($\chi_s\gg1$) which tend to scatter strongly in the forward direction (Fig. 6d–f). However, the use of the HG phase function has been shown to be sufficiently accurate for radiation transfer analysis through strongly forward scattering media such as microalgae suspensions containing gas bubbles [66], glass containing bubbles [71], red blood cells [72,73], and also in the field of ocean optics [74,75].

Note that microalgae cells are strongly forward scattering due to their large size compared with the wavelength of photons in the PAR region. In addition, the solution of the radiative transfer equation derived by Pottier et al. [25] based on the two-flux approximation has been shown to offer a relatively accurate method for predicting the fluence rate in open pond and flat-plate PBRs [25,67].

Their analytical expression requires only the absorption and scattering cross-sections, the microorganism concentration, as well as the backward scattering ratio b of the microalgae suspension. The insets to Fig. 6a–e show the values of b for each aggregate estimated using the scattering phase function predicted using (i) the T-matrix method, (ii) the coated sphere approximation, (iii) the RDG approximation, and (iv) the HG phase function. They indicate that the backward scattering ratio predicted using the coated sphere approximation was within 30% of that predicted by the T-matrix method for aggregates composed of monomers of size parameter $\chi_s = 1$. In addition, b was negligibly small for aggregates composed of monomers with $\chi_s = 5$.

Moreover, Berberoğlu et al. [66] used the discrete ordinates method with a combination of two Gauss quadrature having 24 discrete directions per hemisphere to predict the fluence rate in PBRs containing microorganisms. Results obtained using the HG approximate phase function were in good agreement with those obtained using the phase function predicted by the Lorenz–Mie theory of the microorganism suspension. This demonstrates that for the purposes of unpolarized radiation transfer analysis through microalgae cultures, or any other strongly forward scattering media, knowledge of the integral radiation characteristics $\langle C^a_{abs}\rangle, \langle C^a_{sca}\rangle$, g, and b are sufficient.

Finally, the inset to Fig. 6a–e shows the scattering phase function $F_{11}(\Theta = 0^\circ)$ values obtained by (i) the T-matrix method, (ii) for the equivalent coated sphere, (iii) the RDG approximation, and (iv) the HG phase function. This is of particular interest for large aggregates and/or large monomers since most of the scattered radiation energy is concentrated around the forward direction $\Theta = 0^\circ$. Relatively good agreement was found between the values of $F_{11}(0^\circ)$ predicted by the T-matrix approximation and those predicted for the equivalent coated spheres. In fact, the relative error between the predictions of the two methods was less than 13% for all size parameters χ_s and monomer numbers N_s considered. In addition, the value of $F_{11}(\Theta = 0^\circ)$ predicted by the HG approximation was accurate within 15% for aggregates composed of 36 or 100 monomers with size parameter $\chi_s = 1$. However, it overestimated $F_{11}(0^\circ)$ for aggregates composed of monomers with larger size parameter.

4.4. Scattering matrix element ratios

Polarized incident radiation and the scattering matrix elements can be used in remote sensing applications to

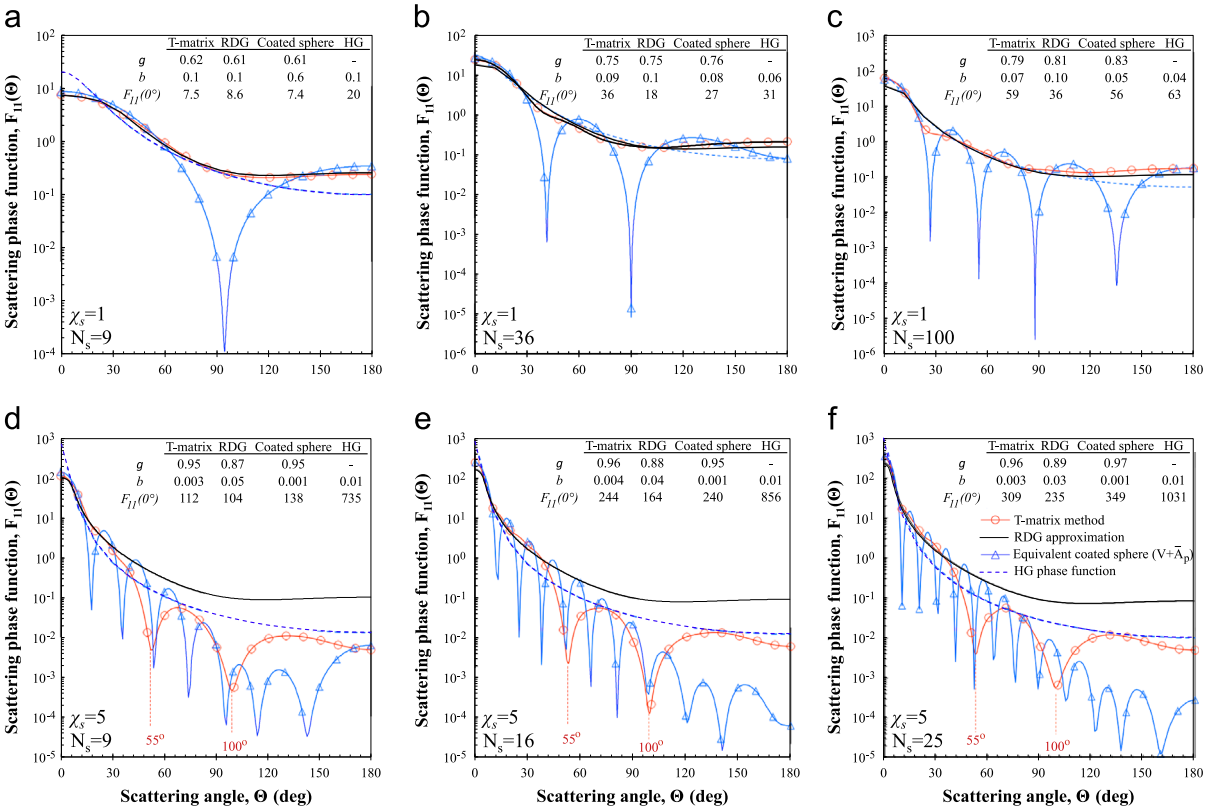

Fig. 6. Scattering phase function $F_{11}(\Theta)$ of randomly oriented aggregates of fractal dimension D_f of 2.25 with monodisperse monomers of size parameters χ_s equal to (a–c) 1.0 or (d–f) 5, $m = 1.0165 + i0.003$ and N_s ranging from 9 to 100 estimated using the superposition T-matrix method, the RDG approximation, and for the volume and average projected area equivalent coated sphere, and the HG phase function. The inset table reports the corresponding asymmetry factor g computed using Eq. (5).

characterize the morphology of the aggregates defined by a, N_s, k_f, D_f, V_T, and/or $\overline{A}_p$.

Fig. 7 plots the normalized scattering matrix element ratios (a) $F_{21}(\Theta)/F_{11}(\Theta)$, (b) $F_{22}(\Theta)/F_{11}(\Theta)$, (c) $F_{33}(\Theta)/F_{11}(\Theta)$, (d) $F_{34}(\Theta)/F_{11}(\Theta)$, and (e) $F_{44}(\Theta)/F_{11}(\Theta)$ predicted by the superposition T-matrix method as functions of scattering angle Θ for randomly oriented aggregates of fractal dimension D_f=2.25 and consisting of 9, 36, and 100 monomers with size parameter χ_s=1 and $m=1.0165+i0.003$. They also show the same scattering matrix element ratios predicted for the volume and average projected area equivalent coated sphere. The degree of linear polarization of the aggregates $F_{21}(\Theta)/F_{11}(\Theta)$ was identical for all values of N_s considered. It reached 100% at scattering angle $\Theta=90^\circ$ and was equal to 0% at scattering angles Θ of 0° and 180°. The scattering matrix element ratio $F_{22}(\Theta)/F_{11}(\Theta)$ was equal to 100% for all scattering angles Θ. The scattering matrix element ratios $F_{33}(\Theta)/F_{11}(\Theta)$ and $F_{44}(\Theta)/F_{11}(\Theta)$ were equal for all aggregates and decreased from 100% at $\Theta=0^\circ$ to −100% at $\Theta=180^\circ$. Finally, the scattering matrix element ratio $F_{34}(\Theta)/F_{11}(\Theta)$ was equal to zero for all angles Θ. Results for the different scattering matrix element ratios presented in Fig. 7 for $\chi_s=1$ were identical to those for a single sphere. This indicates the dominant role of single scattering by the constituent monomers [53,76]. These results confirm the findings by Liu and Mishchenko [53] who demonstrated that increasing the aggregate number of monomers N_s up to 400, with size parameter $\chi_s=0.2$, did not modify the scattering matrix element ratios.

The equivalent coated sphere featured scattering element ratios with overall trends similar to those predicted by the T-matrix method. However, they also featured resonance peaks at scattering angles Θ corresponding to those observed in the scattering phase function shown in Fig. 6a–c and attributed to internal reflectance in the coating. These results indicate that the volume and average projected area equivalent coated sphere approximation cannot be used for predicting the scattering matrix elements of the actual fractal aggregates. Thus, it will not be considered further in this section.

Fig. 8 shows the scattering matrix element ratios (a) $F_{21}(\Theta)/F_{11}(\Theta)$, (b) $F_{22}(\Theta)/F_{11}(\Theta)$, (c) $F_{33}(\Theta)/F_{11}(\Theta)$, (d) $F_{34}(\Theta)/F_{11}(\Theta)$, and (e) $F_{44}(\Theta)/F_{11}(\Theta)$ predicted by the superposition T-matrix method as a function of scattering angle Θ for randomly oriented aggregates of fractal dimension D_f of 2.25 and consisting of 9, 36, and 100 monomers of size parameter χ_s=5 and $m=1.0165+i0.003$. All scattering matrix element ratios featured resonance peaks at scattering angles Θ of 55° and 100° also observed in the aggregate scattering phase function $F_{11}(\Theta)$ (Fig. 6d–f). These resonance peaks appeared in the scattering matrix elements for large enough monomer size parameter. Similar resonance peaks were observed in the scattering matrix element ratios of aggregates composed of linear chain of spheres with size parameter of 10 [34] and for fractal soot aggregates with

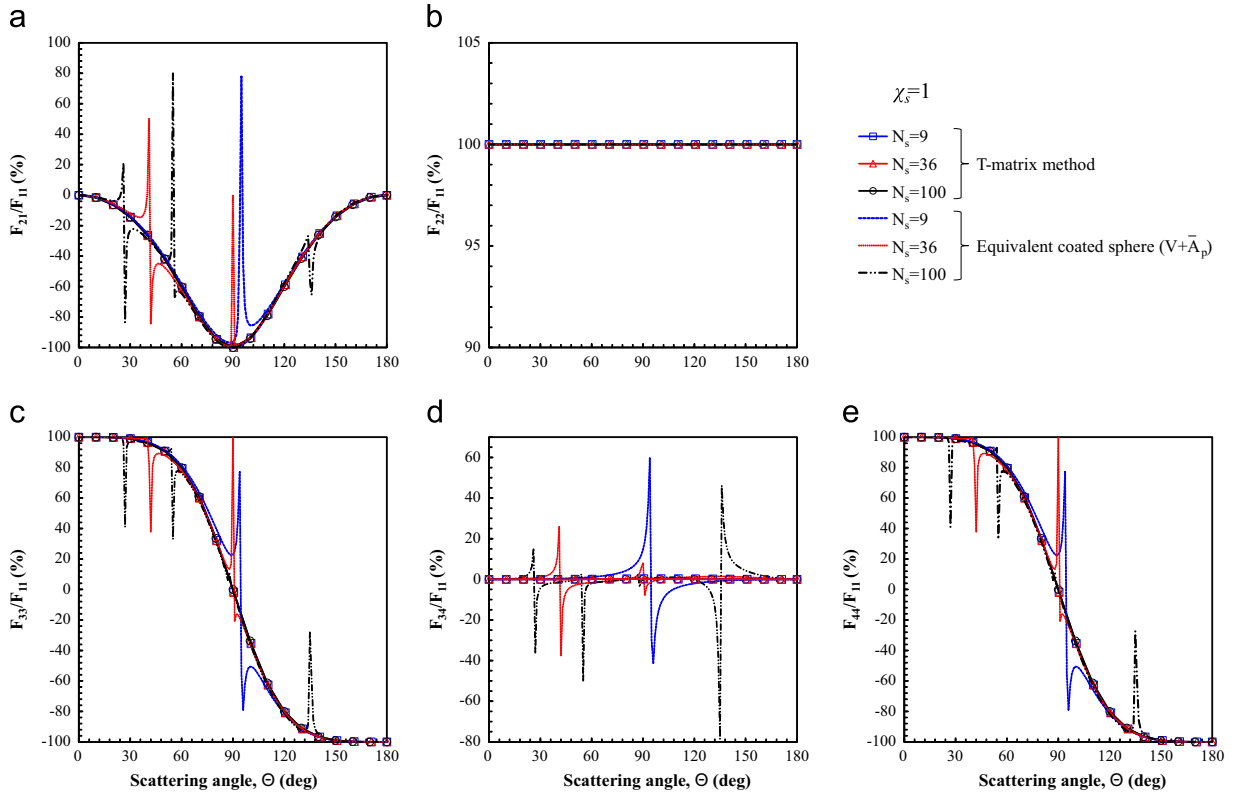

Fig. 7. Scattering matrix element ratios (a) $F_{21}(\Theta)/F_{11}(\Theta)$, (b) $F_{33}(\Theta)/F_{11}(\Theta)$, (c) $F_{34}(\Theta)/F_{11}(\Theta)$, and (d) $F_{44}(\Theta)/F_{11}(\Theta)$ of randomly oriented aggregates with fractal dimension D_f=2.25 containing 9, 36, and 100 monodisperse monomers with size parameter $\chi_s=1$ and relative complex index of refraction $m=1.0165+i0.003$ predicted using the superposition T-matrix method and the volume and average projected area equivalent coated sphere approximation.

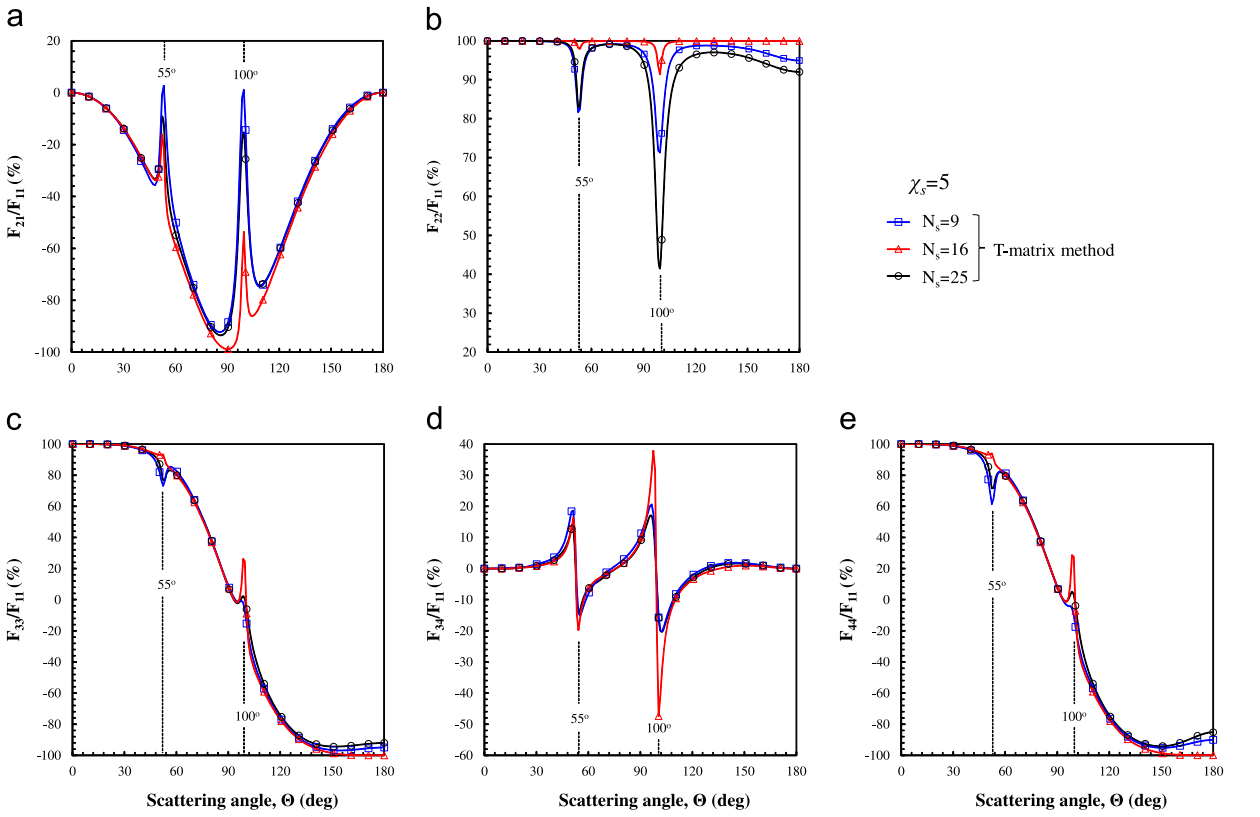

Fig. 8. Scattering matrix element ratios (a) $F_{21}(\Theta)/F_{11}(\Theta)$, (b) $F_{22}(\Theta)/F_{11}(\Theta)$, (c) $F_{33}(\Theta)/F_{11}(\Theta)$, (d) $F_{34}(\Theta)/F_{11}(\Theta)$, and (e) $F_{44}(\Theta)/F_{11}(\Theta)$ of randomly oriented aggregates with fractal dimension D_f=2.25 containing 9, 16, and 25 monodisperse monomers with size parameter $\chi_s = 5$ and $m = 1.0165 + i0.003$ predicted using the superposition T-matrix method.

D_f= 1.82 and k_f= 1.19 composed of 200 monomers with size parameter $\chi_s = 0.6$ [53]. Here, the number and angles of the resonance peaks depended on the monomer size parameter χ_s while their magnitude depended on the number of monomers N_s in the aggregates. Indeed, the scattering matrix element ratios had 1, 2, or 6 resonance peaks for aggregates composed of N_s=9 monomers with size parameter 2.5, 5, or 10, respectively (see Supplementary Materials). These confirm and expand on previous results reported by Mackowski and Mishchenko [77] illustrating that the resonance angles of aggregates of up to 5 spherical monomers of size parameter $\chi_s = 5$ were equal to those for a single sphere of the same size parameter. The authors also reported that increasing monomer number in an aggregate causes "damping of the oscillation in the matrix elements" [77]. However, here no such effect could be observed (see Supplementary Materials).

Furthermore, the ratio $F_{21}(\Theta)/F_{11}(\Theta)$ deviated from unity while the scattering element ratios $F_{33}(\Theta)/F_{11}(\Theta)$ and $F_{44}(\Theta)/F_{11}(\Theta)$ featured similar trends but were not identical. Divergence of the ratio F_{22}/F_{11} from unity as well as the inequality between the ratios F_{33}/F_{11} and F_{44}/F_{11} was also observed by Mishchenko et al. [78] and used as indicators for nonsphericity of randomly oriented bispheres of size parameter $\chi_s = 5$ and relative index of refraction $m = 1.5 + 0.005$. Such features of the scattering matrix elements can be used for remote sensing applications.

5. Conclusion

This study demonstrated that the absorption $\langle C^a_{abs} \rangle$ and scattering $\langle C^a_{sca} \rangle$ cross-sections and the asymmetry factor g of randomly oriented fractal aggregates consisting of spherical monomers can be rapidly estimated as those of coated spheres with equivalent volume and average projected area. Predictions for $\langle C^a_{abs} \rangle$ and $\langle C^a_{sca} \rangle$, and g fell within 8%, 29%, and 15%, respectively, for aggregates composed of monodisperse and polydisperse monomers with (i) size parameter χ_s between 0.01 and 20, (ii) number N_s ranging from 1 to 1000, (iii) relative refractive index of 1.0165 and absorption index varying from 0.003 to 0.5, and (iv) for aggregates of fractal dimension ranging from 2.0 to 3.0. First, a convenient correlation was derived for the average projected area of fractal aggregates with various fractal dimensions. The proposed equivalent coated sphere approximation was able to capture multiple scattering in the aggregates and shading among constituent monomers on the integral radiation characteristics of the aggregate. It was also superior to that proposed by Latimer [57] and to the Rayleigh–Debye–Gans approximation, particularly for large values of χ_s and N_s. In addition, the use of Henyey–Greenstein approximate phase function estimated using the asymmetry factor for the equivalent coated sphere yielded acceptable predictions of the actual aggregate scattering phase function for all values of χ_s and N_s considered.

However, the equivalent coated spheres featured scattering matrix element ratios significantly different from those of the aggregates due to internal reflection in the coating. Finally, the scattering phase function and the scattering matrix elements were found to have unique features for large monomer size parameter χ_s. These could be used in remote sensing applications to measure the morphology of such aggregates.

Acknowledgments

This research was supported in part by the U.S. NSF-IGERT program Clean Energy for Green Industry at UCLA (DGE-0903720). Computation was performed on the Hoffman 2 cluster hosted by the Academic Technology Services at the University of California, Los Angeles.

Appendix A. Supplementary data

Supplementary data associated with this paper can be found in the online version at http://dx.doi.org/10.1016/j.jqsrt.2014.10.018.

References

[1] Liou KN, Takano Y, Yang P. Light absorption and scattering by aggregates: application to black carbon and snow grains. J Quant Spectrosc Radiat Transf 2011;112(10):1581–94.
[2] Sorensen CM. Light scattering by fractal aggregates: a review. Aerosol Sci Technol 2001;35(2):648–87.
[3] Takano Y, Liou KN, Kahnert M, Yang P. The single-scattering properties of black carbon aggregates determined from the geometric-optics surface-wave approach and the T-matrix method. J Quant Spectrosc Radiat Transf 2013;125:51–6.
[4] Kimura H, Kolokolova L, Mann I. Optical properties of cometary dust. Astron Astrophys 2003;407(1):L5–8.
[5] Norman TJ, Grant CD, Maganaand D, Zhang JZ, Liu J, et al. Near infrared optical absorption of gold nanoparticle aggregates. J Phys Chem B 2002;106(28):7005–12.
[6] Guan J, Waite TD, Amal R, Bustamante H, Wukasch R. Rapid determination of fractal structure of bacterial assemblages in wastewater treatment: implications to process optimisation. Water Sci Technol 1998;38(2):9–15.
[7] Jiang Q, Logan BE. Fractal dimensions of aggregates determined from stead-state size distribution. Environ Sci Technol 1991;25(12):2031–8.
[8] Jackson GA, Maffione R, Costello DK, Alldredge AL, Logan BE, Dam HG. Particle size spectra between 1 μm and 1 cm at Monterey Bay determined using multiple instruments. Deep Sea Res Part I: Oceanogr Res Pap 1997;44(11):1739–67.
[9] Friedlander S, Sioutas C. Final report: measurement of the effective surface area of ultrafine and accumulation mode PM (pilot project). Technical report R827352, United States Environmental Protection Agency, Los Angeles, CA; 2006.
[10] Electron and Agricultural Research Service Confocal Microscopy Laboratory, Rime and Graupel, United States Department of Agriculture, Beltsville, MD ⟨http://emu.arsusda.gov/snowsite/rimegraupel/rg.html⟩, 2006.
[11] Jet Propulsion Laboratory, A 10 micron interplanetary dust collected in the stratosphere, National Aeronautic and Space Administration, Pasadena, CA ⟨http://stardust.jpl.nasa.gov/science/sd-particle.html#idp-s⟩, 2003.
[12] F.D.A. Keene, Clusters of roughly 30-nanometer gold nanoparticles imaged by transmission electron microscopy, National Institute of Standards and Technology, Gaithersburg, MD ⟨http://www.nist.gov/mml/biochemical/cluster-102511.cfm⟩, 2011.
[13] Carr J. *Micrococcus luteus* 9757, centers for disease control and prevention: public health image library, Atlanta, GA; 2007
[14] Brennan L, Owende P. Biofuels from microalgae: a review of technologies for production, processing, and extractions of biofuels and co-products. Renew Sustain Energy Rev 2010;14(2):557–77.
[15] Dayananda C, Sarada R, Usha Rani M, Shamala TR, Ravishankar GA. Autotrophic cultivation of *Botryococcus braunii* for the production of hydrocarbons and exopolysaccharides in various media. Biomass Bioenergy 2007;31(1):87–93.
[16] Demura M, Ioki M, Kawachi M, Nakajima N, Watanabe M. Desiccation tolerance of *Botryococcus braunii* (trebouxiophyceae, chlorophyta) and extreme temperature tolerance of dehydrated cells. J Appl Phycol 2014;26(1):49–53.
[17] Díaz Bayona KC, Atehortúa Garcés L. Effect of different media on exopolysaccharide and biomass production by the green microalgae *Botryococcus braunii*. J Appl Phycol 2014;26(5):2087–95. http://dx.doi.org/10.1007/s10811-014-0242-5.
[18] Souliés A, Pruvost J, Legrand J, Castelain C, Burghelea TI. Rheological properties of suspensions of the green microalga *Chlorella vulgaris* at various volume fractions. Rheol Acta 2013;52(6):589–605.
[19] Cornet J-F, Dussap C-G. A simple and reliable formula for assessment of maximum volumetric productivities in photobioreactors. Biotechnol Prog 2009;25(2):424–35.
[20] Pilon L, Berberoğlu H, Kandilian R. Radiation transfer in photobiological carbon dioxide fixation and fuel production by microalgae. J Quant Spectrosc Radiat Transf 2011;112(17):2639–60.
[21] Pruvost J, Cornet J-F. Knowledge models for the engineering and optimization of photobioreactors. In: Posten C, Walter C, editors. Microalgal biotechnology. Berlin, Germany: De Gruyter; 2012. p. 181–224.
[22] Takache H, Pruvost J, Cornet J-F. Kinetic modeling of the photosynthetic growth of *Chlamydomonas reinhardtii* in a photobioreactor. Biotechnol Progr 2012;28(3):681–92.
[23] Jonasz M, Fournier G. Light scattering by particles in water: theoretical and experimental foundations. San Diego, CA: Academic Press; 2007.
[24] Stramski D, Morel A, Bricaud A. Modeling the light attenuation and scattering by spherical phytoplanktonic cells: a retrieval of the bulk refractive index. Appl Opt 1988;27(19):3954–6.
[25] Pottier L, Pruvost J, Deremetz J, Cornet JF, Legrand J, Dussap CG. A fully predictive model for one-dimensional light attenuation by *Chlamydomonas reinhardtii* in a torus photobioreactor. Biotechnol Bioeng 2005;91(5):569–82.
[26] Quirantes A, Bernard S. Light-scattering methods for modeling algal particles as a collection of coated and/or nonspherical scatterers. J Quant Spectrosc Radiat Transf 2006;100(1–3):315–24.
[27] Berberoğlu H, Yin J, Pilon L. Light transfer in bubble sparged photobioreactors for H_2 production and CO_2 mitigation. Int J Hydrog Energy 2007;32(13):2273–85.
[28] Davies-Colley RJ. Optical properties and reflectance spectra of 3 shallow lakes obtained from a spectrophotometric study. N Z J Mar Freshw Res 1983;17(4):445–59.
[29] Mackowski DW, Mishchenko MI. A multiple sphere T-matrix Fortran code for use on parallel computer clusters. J Quant Spectrosc Radiat Transf 2011;112(13):2182–92.
[30] Xu Y-L. Electromagnetic scattering by an aggregate of spheres: far field. Appl Opt 1997;36(36):9496–508.
[31] Iskander MF, Chen HY, Penner JE. Optical scattering and absorption by branched chains of aerosols. Appl Opt 1989;28(15):3083–91.
[32] Kahnert M, Nousiainen T, Lindqvist H. Review: model particles in atmospheric optics. J Quant Spectrosc Radiat Transf 2014;146:41–58.
[33] Drolen BL, Tien CL. Absorption and scattering of agglomerated soot particulate. J Quant Spectrosc Radiat Transf 1987;37(5):433–48.
[34] Lee E, Pilon L. Absorption and scattering by long and randomly oriented linear chains of spheres. J Opt Soc Am A 2013;30(9):1892–900.
[35] Farias TL, Köylü ÜÖ, Carvalho MG. Effects of polydispersity of aggregates and primary particles on radiative properties of simulated soot. J Quant Spectrosc Radiat Transf 1996;55(3):357–71.
[36] Sorensen CM, Cai J, Lu N. Light-scattering measurements of monomer size, monomers per aggregate, and fractal dimension for soot aggregates in flames. Appl Opt 1992;31(30):6547–57.
[37] Köylü ÜÖ, Faeth GM, Farias TL, Carvalho MG. Fractal and projected structure properties of soot aggregates. Combust Flame 1995;100(4):621–33.
[38] Farias TL, Köylü ÜÖ, Carvalho MG. Range of validity of the Rayleigh–Debye–Gans theory for optics of fractal aggregates. Appl Opt 1996;35(33):6560–7.
[39] Lapuerta M, Martos FJ, Martín-González G. Geometrical determination of the lacunarity of agglomerates with integer fractal dimension. J Colloid Interface Sci 2010;346(1):23–31.
[40] Mroczka J, Woźniak M, Onofri FRA. Algorithms and methods for analysis of the optical structure factor of fractal aggregates. Metrol Meas Syst 2012;19(3):459–70.

[41] Woźniak M, Onofri FRA, Barbosa S, Yon J, Mroczka J. Comparison of methods to derive morphological parameters of multi-fractal samples of particle aggregates from TEM images. J Aerosol Sci 2012;47:12–26.
[42] Mishchenko MI, Travis LD, Lacis AA. Scattering, absorption, and emission of light by small particles. Cambridge, UK: Cambridge University Press; 2002.
[43] Mackowski DW. A simplified model to predict the effects of aggregation on the absorption properties of soot particles. J Quant Spectrosc Radiat Transf 2006;100(1–3):237–49.
[44] Bohren CF, Huffman DR. Absorption and scattering of light by small particles. New York, NY: Wiley & Sons; 1983.
[45] Modest MF. Radiative heat transfer. San Diego, CA: Academic Press; 2003.
[46] Yang B, Köylü ÜÖ. Soot processes in a strongly radiating turbulent flame from laser scattering/extinction experiments. J Quant Spectrosc Radiat Transf 2005;93(1–3):289–99.
[47] Wang G, Sorensen CM. Experimental test of the Rayleigh–Debye–Gans theory for light scattering by fractal aggregates. Appl Opt 2002;41(22):4645–51.
[48] Bushell G. Forward light scattering to characterize structure of flocs composed of large particles. Chem Eng J 2005;111(23):145–9.
[49] Liu F, Wong C, Snelling DR, Smallwood GJ. Investigation of absorption and scattering properties of soot aggregates of different fractal dimension at 532 nm using RDG and GMM. Aerosol Sci Technol 2013;47(12):1393–405.
[50] Liu F, Snelling DR, Smallwood GJ. Effects of the fractal prefactor on the optical properties of fractal soot aggregates. In: ASME 2009 2nd Micro/Nanoscale Heat & Mass Transfer International Conference, Shanghai, China; 2009, MNHMT2009-18473.
[51] Yurkin MA, Hoekstra AG. The discrete dipole approximation: an overview and recent developments. J Quant Spectrosc Radiat Transf 2007;106:558–89.
[52] Manickavasagam S, Mengüç MP. Scattering matrix elements of fractal-like soot agglomerates. Appl Opt 1997;36(6):1337–51.
[53] Liu L, Mishchenko MI. Effects of aggregation on scattering and radiative properties of soot aerosols. J Geophys Res Atmos 2005;110(D11211).
[54] Liu L, Mishchenko MI. Scattering and radiative properties of complex soot and soot-containing aggregate particles. J Quant Spectrosc Radiat Transf 2007;106(1–3):262–73.
[55] Liu L, Mishchenko MI, Arnott WP. A study of radiative properties of fractal soot aggregates using the superposition T-matrix method. J Quant Spectrosc Radiat Transf 2008;109(15):2656–63.
[56] Dlugach JM, Mishchenko MI, Mackowski DW. Numerical simulations of single and multiple scattering by fractal ice clusters. J Quant Spectrosc Radiat Transf 2011;112(11):1864–70.
[57] Latimer P. Experimental tests of a theoretical method for predicting light scattering by aggregates. Appl Opt 1985;24(19):3231–9.
[58] Bricaud A, Bedhomme AL, Morel A. Optical properties of diverse phytoplanktonic species: experimental results and theoretical interpretation. J Plankton Res 2008;10(8):51–73.
[59] Morel A, Ahn YH. Optics of heterotrophic nanoflagellates and ciliates: a tentative assessment of their scattering role in oceanic waters compared to those of bacterial and algal cells. J Mar Res 1991;49:177–202.
[60] Lee E, Heng R-L, Pilon L. Spectral optical properties of selected photosynthetic microalgae producing biofuels. J Quant Spectrosc Radiat Transf 2013;114:122–35.
[61] Skorupski K, Mroczka J, Wriedt T, Riefler N. A fast and accurate implementation of tunable algorithms used for generation of fractal-like aggregate models. Physica A: Stat Mech Appl 2014;404:106–17.
[62] Heng R-L, Sy KC, Pilon L. Absorption and scattering by bispheres, quadspheres, and circular rings of spheres and their equivalent coated spheres. J Opt Soc Am A 2015;32(1), accepted.
[63] Mätzler C. MATLAB functions for Mie scattering and absorption, version 2, Institut für Angewandte Physik, Bern, Switzerland, report no. 2002-11, 2002.
[64] Kandilian R, Lee E, Pilon L. Radiation and optical properties of *Nannochloropsis oculata* grown under different irradiances and spectra. Bioresour Technol 2013;137:63–73.
[65] Heng R-L, Lee E, Pilon L. Radiation characteristics and optical properties of filamentous cyanobacterium *Anabaena cylindrica*. J Opt Soc Am A 2014;31(4):836–45.
[66] Berberoğlu H, Yin J, Pilon L. Light transfer in bubble sparged photobioreactors for H_2 production and CO_2 mitigation. Int J Hydrog Energy 2007;32(13):2273–85.
[67] Lee E, Pruvost J, He X, Munipalli R, Pilon L. Design tool and guidelines for outdoor photobioreactors. Chem Eng Sci 2014;116:18–29.
[68] Mishchenko MI. Electromagnetic scattering by particles and particle groups: an introduction. New York, NY: Cambridge University Press.
[69] Kerker M. The scattering of light, and other electromagnetic radiation. New York, NY: Academic Press; 1969.
[70] Mc Kellar BHJ, Box MA. The scaling group of the radiative transfer equation. J Atmos Sci 1981;38:1063–8.
[71] Dombrovski LA, Randrianalisoa J, Baillis D, Pilon L. Use of Mie theory to analyze experimental data to identify infrared properties of fused quartz containing bubbles. Appl Opt 2005;44(33):7021–31.
[72] Hammer M, Yaroslavsky AN, Schweitzer D. A scattering phase function for blood with physiological haematocrit. Phys Med Biol 2001;46(3):65–9.
[73] Friebel M, Roggan A, Mueller G, Meinke M. Determination of optical properties of human blood in the spectral range 250 to 1100 nm using Monte-Carlo simulations with hematocrit-dependent effective scattering phase functions. J Biomed Opt 2006;11(3):034021.
[74] Haltrin VI. One-parameter two-term Henyey–Greenstein phase function for light scattering in seawater. Appl Opt 2002;41(6):1022–8.
[75] Mobley CD, Sundman LK, Boss E. Phase function effects on oceanic light fields. Appl Opt 2002;41(6):1035–50.
[76] West RA. Optical properties of aggregate particles whose outer diameter is comparable to the wavelength. Appl Opt 1991;30(36):5316–24.
[77] Mackowski DW, Mishchenko MI. Calculation of the T-matrix and the scattering matrix for ensembles of spheres. J Opt Soc Am A 1996;13(11):2266–78.
[78] Mishchenko MI, Mackowski DW, Travis LD. Scattering of light by bispheres with touching and separated components. Appl Opt 1995;34(21):4589–99.